Dear Dr. Didenkulova,

Please, find in this document, our response to reviewer 2 in which we have included detailed replies to their comments.
We have re-edited the manuscript, which is included at the end of this document. The changes are highlighted in yellow.

Íñigo Aniel-Quiroga
Corresponding autor

In the author reply, many of the details I requested are given, but a lot of them are not included in the revised manuscript, thus leaving a potential reader with the same questions.

The coupling between the two models and the setup of the IH2VOF should be dealt with in more detail in the revised manuscript. I still see some challenges in the coupling the two models. This, however, can be overcome by stating some of the possible limitations. Please see the detailed comments below.

REPLY: In the following paragraphs, the response to the reviewer detailed comments are given. As highlighted by the reviewer, a number of the comments were answered in the previous response, although not included in the manuscript. Now we have included all of them in the text and we have added the details requested in the previous revision response, and we have tried to efficiently explain both the IH2VOF and the coupling of the 2 models.

Detailed comments:

1) I asked for typical grid sizes in the RANS model. This is given in the reply and I feel this information should be present in the paper.

The discussion detailed in the previous "authors response" has now been added at the end of 2.3.

a. Further the authors state that the model do not allow more than 5499 cells in X. Why is that? Is that a choice of the authors?

The commercial version of the numerical model gives this recommendation. We accepted it after several tests in order to avoid long computational times when creating the database. (This aspect is also included in section 2.3).

b. It is stated that the aspect ratio between x and z was 5. I completely understand the need for such a large aspect ratio, to limit computational time. However, large aspect ratio has, as shown by Jacobsen et al (2012), an impact on the position of the breaking point. Despite this, I still think that IH2VOF handle more accurately the physics of the tsunamis in this region than COMCOT, and thus it is justified. A comment should however be made that such large aspect ratios, might lead to slightly premature breaking.

We agree on this limitation, and it has been included also in the section 2.3.

c. An equation is given for determining delta z. Where does this come from? The effect of it can clearly be seen, and to me it seem a reasonable way of automizing the process. Again, I feel that this information should be present in the revised manuscript.

Thanks a lot for this comment. The equation is a recommendation of the model and it is now explained in the manuscript, making the whole design process clearer.

2) I asked for boundary conditions for IH2VOF model, and the authors replied that a log wall distribution was used. This seem reasonable, but, if the mesh is not graded near the bed, the y+ values must be extremely large potentially putting the value of the first grid point outside the log layer. Please discuss the possible impact of this. Further, please also provide

the wall functions for k and epsilon. Finally, another reference than Lara et al. (2006) should probably be used here, as the turbulence model is not described in this paper.

In addition to Lara et al (2006), we have added now other references that help to understand the IH2VOF turbulence model: Hsu et al (2002); Garcia et al (2004), Lin and Liu (1998, 1999)

In this references, specially in García et al(2004), it is set that the model considers a log-law distribution of the mean tangential velocity in the turbulent boundary layer near the solid boundary, where the values of k (turbulent kinetic energy) and e (dissipation rate of turbulent kinetic energy) can be expressed as functions of the distance *y* from the solid boundary and the mean tangential velocity outside the viscous sublayer. The grids must follow literature validations (Torres et al (2007, 2009), Lara et al (2011)) to set cell dimensions in order to avoid that the first grid point falls out of the log layer.

On the free surface, the zero gradient boundary conditions for both k and e are based on the assumption of no turbulence exchange between the water and air. The equations of the k-ε turbulence transport model are:

Free surface: no flux condition $\frac{\partial k}{\partial \mathrm{n}} = \frac{\partial \varepsilon}{\partial \mathrm{n}} = 0$

Solid wall: log-law turbulent boundary layer for smooth surface $\frac{\overrightarrow{u_n}}{u_*} = \frac{1}{k}\ln(\frac{E u_* y}{\nu})$

Where n is; u is velocity ; y is distance from solid boundary and ν is viscosity

These details regarding turbulence model in IH2VOF have been Included in the introduction of section 2 and in 2.3 in the new version of the manuscript.

3) I asked how the x_cut positions was determined. The authors has given a clear and satisfying answer, but not included this explanation in the revised manuscript. Please do so. Further in the response the authors called the model a LSWE model. I thought it was a NLSW model. If it is a NLSW do not alter anything, but if it is a LSWE model, please justify why this sufficient for the simulations since tsunami close to the shore can definitely be nonlinear.

We have added the previous answer to the new version of the manuscript in 2.4. The model is NLSW. This has been corrected as well.

4) I asked about the position of x_cut in relation to capturing the physics of the tsunami. A figure is added in the reply, but this figure the lines cannot clearly be distinguished and thus is hard to read. Further, I do not feel that this figure answers the question posed. One of the physical features a NLSW model cannot handle, but a VOF model can, is the undular bores. These might show further offshore than x_cut. I understand the practical limitation, but feel that a comment stating that there might be situations where the NLSW model is not properly handling the physics, before the VOF models takes over, is warranted.

We agree. One of the reasons of maximizing the RANS model domain is precisely to avoid those effects. A sentence regarding this limitation has been added to the manuscript in the section 2.4

5) I asked about reflection between the two models. I appreciate what the authors are trying to do, and can see that using the unaltered wave will limit reflection between the models. However, I think that this approach will give difficulties in certain cases. It the beach is steep, the tsunami wave will be reflected entirely, as the steep beach acts more or less like a vertical wall. In this case a standing wave will be present similar to that shown in Madsen and Fuhrman (2009) figure 9a. By using the unaltered waveform this behavior cannot be captured. This should be reflected upon in the revised manuscript.

We think that there is some confusion in this aspect and it is our intention to clarify it in the new version of the manuscript. The effects of the reflection are represented in the flume, both at COMCOT and IH2VOF domains.

The problem arises because in most cases tsunami wavelength is longer than IH2VOF domain, producing that the reflected wave on the beach reach the X-cut position before the incident tsunami wave completely cross this position, aliasing the signal to force the IH2VOF domain. Therefore, to eliminate this aliasing we designed the artifice described on the paper. This artifice is just applied to obtain the forcing wave to be used on the IH2VOF domain. Once the initial wave condition is obtained IH2VOF model is forced, reproducing correctly the reflection process observed on the coast.

The effects of the reflection are then taken into account in the run-up calculation. However, we have not analyzed the evolution of the wave and the interaction among several tsunami reflected waves, since we considered that it is out of the scope of the paper, but an effect like the considered standing wave generation could actually occur, and it would not be captured by the flume. We have added a sentence in the new version of the manuscript to explain this limitation.

6) I asked for more details regarding the calculations for figure 4. These have been provided, but some things are still unclear. Now it is stated that L_i=50/tan(beta_0). How can this be true? In page 10 lines 17-19 it is stated that horizontal length of the domain comes from a separate simulation using COMCOT only.

The design of the flume was carried out by applying the expression L_i=50/tan(beta_0). The formula´s objective is to set a limit of elevation of 50 m in order to define Li and beta_0 from the cut with the profile. Then, in order to maximize the area where VOF model is applied, the run-up is pre-calculated with COMCOT and the VOF domain is moved seawards cover, with a safety factor to prevent that if run-up calculated with IH2VOF is longer that the one calculated with COMCOT, it does not reach the limit of the domain. As a result, the area where VOF model is effectively used (no-cells further than run-up limit) is maximum.

This explanation is included in the section 2.4 of the manuscript.

7) I asked for a validation of the Hybrid model. I fully appreciate that both models have been used with great success in the past, and I did not question the validity of the models. In Lara et al. (2006) however smaller aspect ratios were used compared to here. The additional figure indeed provides validation for that IH2VOF can handle run-up. It is however important that the mesh for these simulations were performed using the same rules as in the present paper. I.e. delta z= (K H)/10 *0.05) *0.05, and r=5/1. Is this the case? If not, I would argue that

the validation is made on a much finer mesh than the simulations in present paper. In this case, I do not feel that the model is validated satisfactory, and new validation simulations should be made.

The accompanying text to the figure is also unclear. In page 13 line 4 it is stated that the validation and coupling of the numerical models was made by comparing to experimental results. In the legend in the figure however, it is only the IH2VOF model, and thus no coupling between the models are present. Which of these are correct?

We appreciate this comment. We realized that the explanation could be a bit confusing.

As highlighted by the reviewer, Lara et al (2006) used smaller ratios than us. The reason for this is that in our case, tsunami problem requires some specific conditions for simulation due to the size of the domain and the wave, in particular the wavelength and period.

The validation process performed was complex:

First, to perform the validation, and due to the difficulties on using lab or real measurements of tsunami wave propagation we compared the results to the available experiments of Synolakis, Baldock, We verified that IH2VOF can reproduce Synolakis and Baldock experiments using the same rules as in the present paper. We have included this information in the paper accordingly.

In addition, we compared the run-up calculated with the numerical flume (COMCOT + IH2VOF) with the result of applying just IH2VOF in the whole geometry. We consider that IH2VOF model solves appropriately the whole domain, and thus the comparison with this performance at scale is an adequate validation. This comparison was depicted in a figure included in our previous “author´s response” and now, a modified and clearer version of it has been included in the new version of the manuscript.

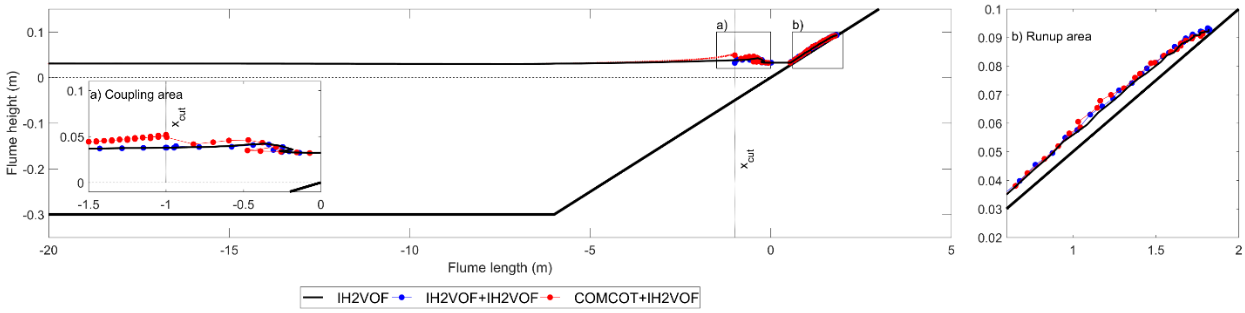

We have modified a paragraph to explain these aspects of the validation process at the end of section 2.

8) The authors have compared now both to Synolakis as well as Madsen and Schaëffer. I am however curious how the results from Synolakis as well as Madsen and Schäeffer were obtained, as these were created for only a single sloped region. Was an average slope calculated? Or only beta_1 or beta_0 used? Please describe how it was done, and why this is the best approach.

The application of these formulae to real geometry is, as the reviewer comments, at least complicated. One of the objectives of these methodology is precisely to overcome these difficulties. The validation of the methodology is made both with numerical models and recorded data. The comparison with Synolakis and Madsen&Schaëffer formulae is not to validate the methodology but to compare with existing alternative approaches.

There are, at first sight, several approaches to apply Synolakis and M&S formulae to our geometries. The direct use, as explained, is not easy, since there is not an *agreement* for their application. We find that the definition of the profile to use in the application of the formulae is complicated, mainly by the assumption of using a single slope to represent a more complex geometry. Considering our geometry, there are several options to apply the formula: using just beta_0, using just beta_1, using an averaged slope of beta_0 and beta_1, using an averaged beta from beta_0_1_2, etc. The use of a unique slope (beta_0 or beta_1) modifies strongly the profile. We studied several options and finally we observed that the approach that calculated the run-up more precisely (closer to the result of the numerical model) was using an averaged profile (from beta_0, beta _1, beta _2). We realize that this approach is not ideal, but it is the one that obtained the best results, and we chose it because we considered it the most coherent and the most restrictive in the comparison.

In the new version of the manuscript it is stated that the calculation with the formulae was made assuming an averaged slope.

9) I asked about the determining of period and wave height. In the reply the authors state that no serious differences between trough led or crest led were experienced. What about difference between a single wave, and a leading depression n-wave for instance. With the N-wave height is the summation of the positive negative amplitude, whereas the wave height of the single wave is just the positive amplitude. I can see how a single wave with a similar positive amplitude as a leading depression N-wave, will run-up similar but I would imagine a single and an N-wave with the same wave height will run-up differently. Perhaps it would be better to called maximum positive amplitude in the revised manuscript rather than wave height.

We agree that the shape of the wave, its height and period, makes the final result to vary. However, as explained, the system itself allows to manually edit this values. In this sense, in order to be strict, in the definition of the height within IHTRUST, in section 4.1, the name of the automatically calculated height has been changed from wave height to maximum positive amplitude.

Tsunami run-up estimation based on a hybrid numerical flume and a parameterization of real topobathymetric profiles

Íñigo Aniel-Quiroga[1], Omar Quetzalcóatl[1], Mauricio González[1], Louise Guillou[1]

[1]Environmental Hydraulics Institute, Universidad de Cantabria - Avda. Isabel Torres, 15, Parque Científico y Tecnológico de Cantabria, 39011, Santander, Spain

Correspondence to: Íñigo Aniel-Quiroga (anieli@unican.es)

Abstract. Tsunami run-up is a key value to determine when calculating and assessing the tsunami hazard in a tsunami-prone area. Run-up can be accurately calculated by means of numerical models, but these models require high-resolution topobathymetric data, which are not always available, and long computational times. These drawbacks restrict the application of these models to the assessment of small areas. As an alternative method, to address large areas, empirical formulae are commonly applied to estimate run-up. These formulae are based on numerical or physical experiments on idealized geometries. In this paper, a new methodology is presented to calculate tsunami hazard at large scales. This methodology determines the tsunami flooding by using a coupled model that combines a nonlinear shallow water model (2D-H) and a volume-of-fluid model (RANS 2D-V) and applies the optimal numerical models in each phase of the tsunami generation-propagation-inundation process. The hybrid model has been widely applied to build a tsunami run-up database (TRD). The aim of this database is to form an interpolation domain with which to estimate the tsunami run-up of new scenarios without running a numerical simulation. The TRD was generated by simulating the propagation of parameterized tsunami waves on real non-scaled profiles. A database and hybrid numerical model were validated using real and synthetic scenarios. The new methodology provides feasible estimations of the tsunami run-up; engineers and scientists can use this methodology to address tsunami hazard at large scales.

1. Introduction

Recent tragic tsunami events, like those that occurred in the Indian Ocean in 2004, in Chile in 2010, and in Japan in 2011 have exposed the need for further work to develop and apply tsunami risk reduction measures. The adequate evaluation of tsunami hazard in tsunami-prone areas is the first step in a proper risk evaluation (UNESCO-IOC, 2009). Determination of the tsunami hazard focuses on the estimation of the area that would be flooded during a tsunami and on the calculation of the variables or parameters that define the phenomenon in that area, e.g., wave amplitude, current depth, tsunami travel time, etc. Among these parameters, maximum run-up provides the elevation to which water from a tsunami wave will rise during its flooding process. Therefore, run-up is a key parameter that must be adequately determined when assessing the inundation of affected areas.

When tsunami hazard is addressed at a local scale (tens of kilometers or one coastal city), the optimal methodology to calculate the flooding and run-up is typically the application of validated deterministic numerical models (Álvarez-Gómez et al., 2013; Titov et al., 2011; Wang, 2009). These models allow reproduction of the 3 main tsunami processes: generation, propagation and inundation. To address these processes and to properly estimate the flooded area, high-resolution topography-bathymetry data of the study area are required, as well as the focal parameters that define the tsunamigenic mechanism. Nevertheless, the application of tsunami numerical models has some limitations and uncertainties (Park et al., 2015; Selva et al., 2016). First, their use requires a high computational cost and expert modelers. Second, the necessary high-resolution data to properly study the hazard in local areas are not always available. In addition, the correct definition of the tsunamigenic mechanisms, e.g., the parameters of the focal mechanism, contains uncertainties in itself. Finally, even though models are evolving to reduce uncertainties, there is still ongoing work on several aspects, such as wave transformation near the coast, interaction of waves with coastal structures, and accurate incorporation of bottom friction.

On the other hand, in large-scale studies (hundreds of kilometers or the coast of a whole country), the drawbacks of numerical models are more evident, and the lack of continuous high-resolution topobathymetry and the elevated computational cost foster the use of other approaches. An alternative methodology to estimate the tsunami run-up and, consequently, the flooded area, includes the application of run-up analytical or empirical formulae. In these cases, numerical models, despite the lower resolution of bathymetry, adequately calculate the tsunami wave characteristics offshore and can then be used as input for the formulae. Afterwards, by applying this method to several topobathymetric profiles along the coast, the total flooded area due to tsunami action can be estimated.

The calculation and analysis of run-up was initially approached by Carrier and Greenspan (1958). They found the exact solution for the nonlinear shallow water equations for a sloping beach with non-breaking regular waves. Keller and Keller (1964) derived an analytical solution for linear shallow water waves at a constant depth moving up a constant slope beach. This geometry has become the canonical problem. Synolakis (1987) extended Carrier and Greenspan's result to this problem by joining Carrier and Greenspan's and Keller and Keller 's solutions to provide a closed-form solution for solitary wave run-up. Synolakis' results are remarkable, as solitary waves have been widely used to model tsunamis, numerically and physically. Li and Raichlen (2001) revisited Synolakis’s results to determine the importance of a higher order correction to the analytical approach. Later, Madsen et al. (2008) demonstrated that solitary waves do not represent the large scale of a tsunami, and Chan and Liu (2012) confirmed this affirmation. Madsen and Schäffer (2010) found closed-form solutions for the run-up of waves of several shapes; their solutions included other parameters, such as the period, achieving more realistic results. Finally, (Fuentes et al., 2015) studied the run-up on multilinear sloping beaches.

In addition, run-up has been commonly linked with the Iribarren number (Iribarren and Nogales, 1949), also called the surf similarity parameter (Battjes, 1974). Hunt (1959) joined this parameter with the non-dimensional run-up of regular waves.

Kobayashi and Karjadi (1994) combined physical and numerical simulations to derive an equation to calculate run-up, using the ratio between the run-up and the wave amplitude and its relationship with the surf-similarity parameter. Fuhrman and Madsen (2008) demonstrated that the relationship between surf-similarity and solitary waves was similar to the that between surf-similarity and period waves.

More recently, several authors have focused their work on calculating tsunami run-up by developing new models with other approaches. Sepúlveda and Liu (2016) presented expressions for the calculation of the run-up based on the parameters that defined the focal mechanism of the tsunamigenic seism. Riquelme et al. (2015) derived simple solutions to estimate run-up on nearfield tsunamis by extending Synolakis solution (Synolakis, 1987) and Park et al. (2015) defined the run-up for compound slopes, based on the work of Madsen and Schäffer (2010) and numerical simulations of tsunami waves on two-slope topobathymetric profiles.

However, the application of these equations and formulae is not always evident, and each approach considers different inputs. Moreover, the parameterization presented by Carrier and Greenspan (1958), extended by Synolakis (1987) and modified by Park et al. (2015), is based on theoretical bathymetric profiles. It does not explicitly consider real profiles or the geometry of the whole area, from the tsunami generation zone to the flooded area. Furthermore, the numerical models that do consider the natural geometry of the bathymetric profiles adequately predict propagation, but they cannot accurately solve the flooding calculation, in addition to the other exposed drawbacks.

Complementing these methodologies, this work presents an alternative methodology to calculate tsunami flooding at large scales and is focused on assessing the run-up. The methodology is then applied to further develop a database from which the tsunami run-up of new scenarios can be interpolated.

The main component of the methodology is a numerical flume where the simulations are run. This flume was developed by combining a nonlinear shallow-water-equations model and a Navier-Stokes volume-of-fluid model to create a hybrid model that applies the optimal numerical model in each area of the flume. Time series of tsunami waves and topobathymetric profiles are used as input to calculate the run-up.

This hybrid model has been applied to further develop a database from which the run-up of new tsunami scenarios can be interpolated. This database contains an adequate representation of natural bathymetric profiles worldwide and the variability in tsunami wave shapes, allowing calculation of the tsunami run-up of new scenarios by interpolation without running a numerical simulation.

The aim of this methodology is to help specialists to further develop tsunami hazard maps at large scales, where the application of numerical models is not computationally affordable and high-resolution data are not available. This method can be used to quickly estimate the run-up in tsunami-prone areas or accurately estimate the flooded area for new tsunami scenarios.

The paper is structured as follows: Section 2 describes the developed methodology, including the parameterization of realistic bathymetric profiles and tsunami wave shapes and the construction of the numerical flume. In section 3, the application of the methodology to calculate the tsunami run-up database is discussed, together with a sensitivity analysis of the influence of each parameter on the final value of the run-up. Section 4 includes details of the tool that has been developed in order to use the database to calculate new tsunami event run-ups. Section 5 presents the validation of the methodology with real and numerical scenarios. Finally, section 6 discusses the conclusions drawn from this work.

2. Tsunami run-up hybrid model methodology

The run-up calculation methodology presented in this paper consists of the numerical simulation of tsunami waves along real non-scaled bathymetric profiles that were previously parameterized.

To carry out these simulations, a numerical flume was designed. This flume is formed by the coupling of two numerical models.

The Cornell Multi-grid Coupled Tsunami Model (COMCOT, (Wang, 2009)) solves the nonlinear shallow water equations (NLSWE) using a leap-frog finite differences scheme on a 2D horizontal domain. In addition, the IH2VOF model (Lara et al., 2006) solves volume-averaged Reynolds-averaged Navier-Stokes (VARANS) equations based on the decomposition of the velocity and pressure fields into mean and turbulent components using a k-ε turbulent model on a 2D vertical domain, using a log-law distribution of the mean tangential velocity in the turbulent boundary layer near the solid boundary, where the values of k (turbulent kinetic energy) and ε (dissipation rate of turbulent kinetic energy) can be expressed as functions of the distance y from the solid boundary and the mean tangential velocity outside the viscous sublayer. (Garcia et al., 2004; Hsu et al., 2002; Lara et al., 2006; Lin and Liu, 1998; Pengzhi Lin and L-F Liu, 1999). On the free surface, the zero gradient boundary conditions for both k and ε are based on the assumption of no turbulence exchange between the water and air. The equations of the k-ε turbulence transport model are:

Free surface: no flux condition $\frac{\partial \mathrm{k}}{\partial n} = \frac{\partial \varepsilon}{\partial n} = 0$

Solid wall: log-law turbulent boundary layer for smooth surface $\frac{\overrightarrow{u_n}}{u_*} = \frac{1}{K}\ln(\frac{E u_* y}{\nu})$

where n is the unit normal on the free surface, K is the von Karman constant, y is the distance from the solid domain and u_* is a friction velocity.

COMCOT model is prepared to simulate the stages of tsunami propagation; meanwhile, IH2VOF model is specially designed to simulate the coastal processes and wave transformations present when the waves reach the coastal areas. IH2VOF model calculates the run-up by evaluating the water accumulated in each column of the grid, tracking the changes on each cell density.

In the flume, the strengths of both models are used to design a numerical space where tsunami waves are propagated, using COMCOT from the deep ocean (~4 km depth) to the coast, where the capabilities of the IH2VOF model are applied to calculate the flooding. As a result, a hybrid model that adequately solves the tsunami processes in both deep and shallow waters was achieved.

Parameterized profiles and a tsunami wave time series dataset are used as input for the numerical flume. These inputs, the most relevant aspects of the numerical flume geometry, and the coupling of the models are described below.

2.1 Bathymetric profile characterization

Worldwide bathymetric profiles were analyzed, with a focus on finding a parameterization that properly represents natural shapes.

To cover the existing variability in the world bathymetry, a representative sample of 50 averaged profiles was obtained from tsunami-prone coastal areas and basins, namely, the Pacific Ocean, Indian Ocean, Mediterranean Sea and Caribbean Sea (Fig. 1). Topographic and bathymetric information was obtained from the General Bathymetric Chart of the Oceans (GEBCO, International Hydrographic Organization, 2014, with a cell size Δx=30”), The European Marine Observation and Data Network (Bathymetry Consortium EMODnet, 2016) and the local bathymetry data that was available. The shape of these profiles was analyzed to perform an adequate parameterization.

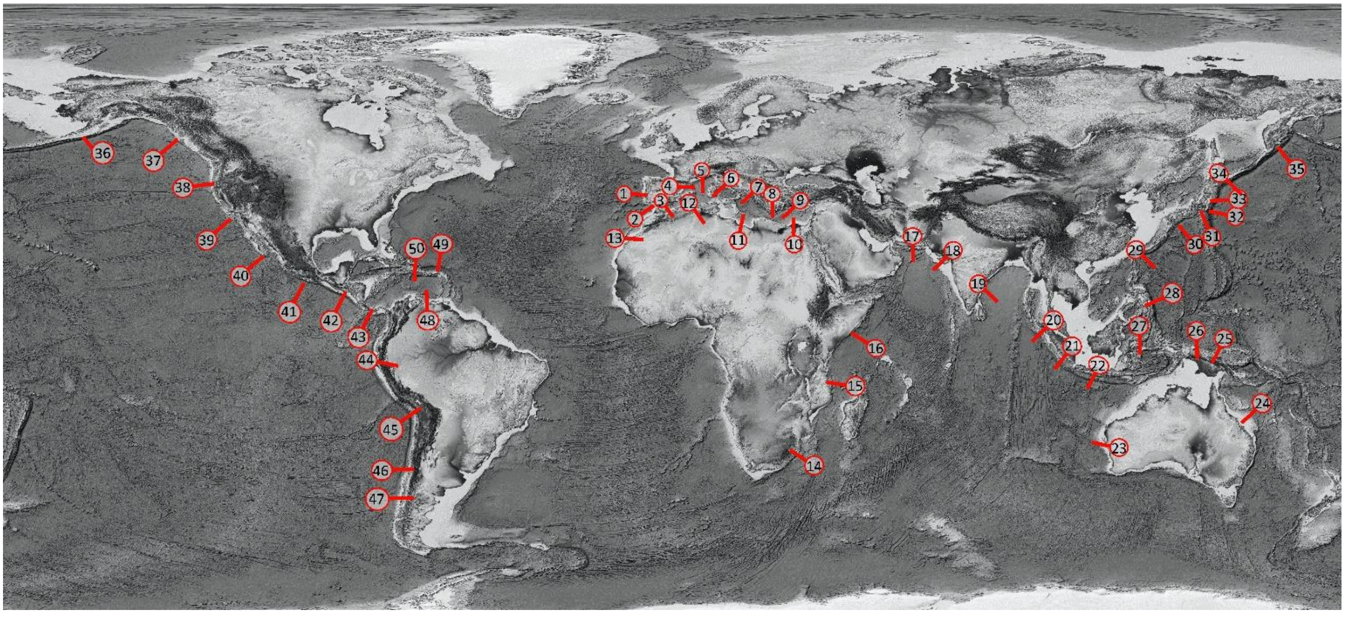

Fig. 1. Distribution of sample profiles

The propagation of a tsunami can affect thousands of kilometers; thus, the profiles must extend under both deep water and shallow water to capture tsunami generation to flooding. Considering this requirement, profiles were defined from inland (50 m height) to the deep ocean (~4000 m depth). To avoid singularities, each defined profile is the average profile of a 10-km-wide coastal segment. Based on the bathymetric shapes observed in this selection, a representative and functional parameterization the profiles was tackled, using five parameters: three slopes (tan $\beta_{1,}$ tan $\beta_{2,}$ and tan β_3) and two depths (d_1 and d_2). Fig. 2 shows the five-parameter geometry.

As an example, in Fig. 3, a selected profile from the Indonesian coast is shown, as well as its parameterized profile that was created by applying the five-parameter geometry. The parameters for each considered profile were fitted by using a least-squares method.

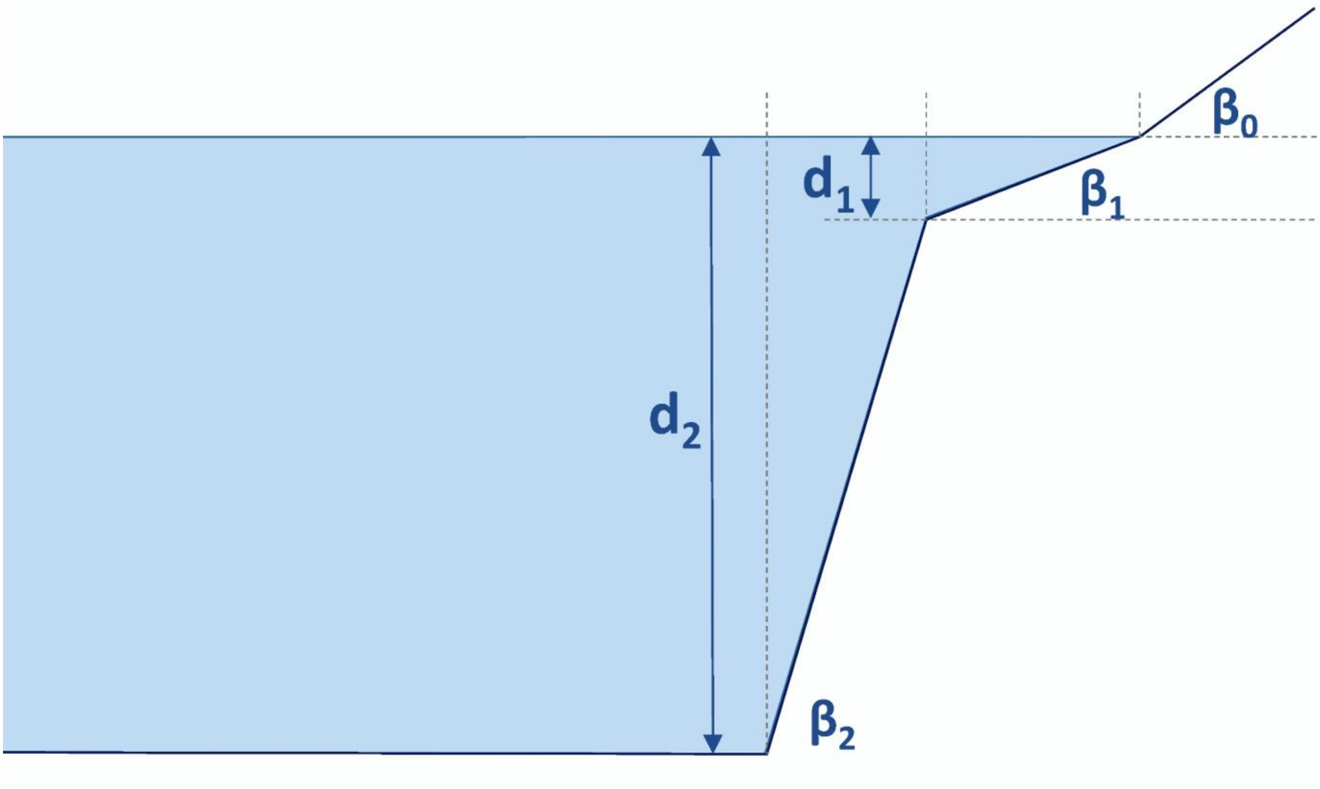

Fig. 2. Scheme of the parameterized profiles, based on real profiles analyses. The profiles are defined by 3 angles (tan β_1, tan β_2, and tan β_3) and 2 depths (d_1 and d_2)

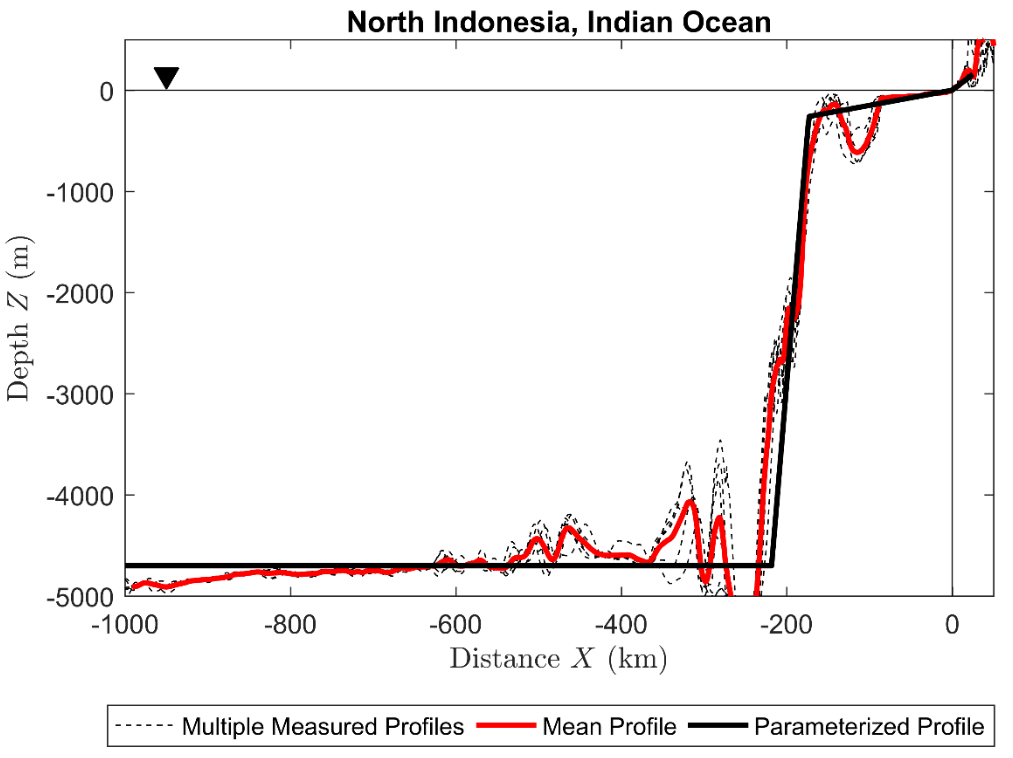

Fig. 3. Sample of measured topobathymetric profiles on the Indonesian coast, as well as the mean and parameterized profiles. GEBCO was used as source for the topobathymetric data (Cell size Δx=30")

The maximum and minimum values of the 5 parameters are shown in Table 1. These values cover a wide range of the profiles that can be found in nature. Despite not including all the existing geometries, the maximum and minimum values certainly provide enough information to characterize the topobathymetric profiles.

Table 1. Maximum and minimum values of the profile parameters

Parameter	Min	Max
d_1	20 m	1100 m
d_2	2200 m	6000 m
$\tan\beta_0$	$5.0e^{-4}$	$1.5e^{-1}$
$\tan\beta_1$	$5.0e^{-4}$	$2.5e^{-2}$
$\tan\beta_2$	$1.0e^{-2}$	$2.0e^{-1}$

2.2 Initial tsunami wave characterization

The numerical flume described in detail in the next subsection requires not only the topo-bathymetric profile characterization but also the characteristics of the tsunami waves as input. To use these data as input for the hybrid model, a time series of the offshore wave amplitude must be provided. These time series could be obtained from either records of real tsunamis, e.g., from DART buoys, or from the results of numerical model tsunami propagation. In this case, COMCOT (Wang, 2009) was adopted. This model calculates all stages of tsunami modeling (generation, propagation and coastal flooding).

The generation of the tsunamis in COMCOT is approached via elastic finite fault plane theory, using the so-called Okada model (Okada, 1985). This model assumes an idealized rectangular fault plane as a representation of two colliding tectonic plates. The Okada model requires 7 focal mechanism parameters as input to calculate the initial deformation of the water surface due to the earthquake. These parameters are the focal depth (h_{focal}), rupture length (L) and width (W) of the fault plane, dislocation (D), strike direction (θ), dip angle (δ) and slip (rake) angle (λ). An instantaneous tsunami generation with a constant distribution of the slip is assumed. A simulation of the numerical model provides the wave amplitude time series to be used as input for the hybrid model.

2.3 Numerical flume geometry

The dimensions of the numerical flume vary with the profile characteristics, adapting the domain for each simulation. The geometry of the flume is shown in Fig. 4. The total length L of the flume is split in two components: L_{off} is the submerged part of the profile and L_i is the inland part of the profile.

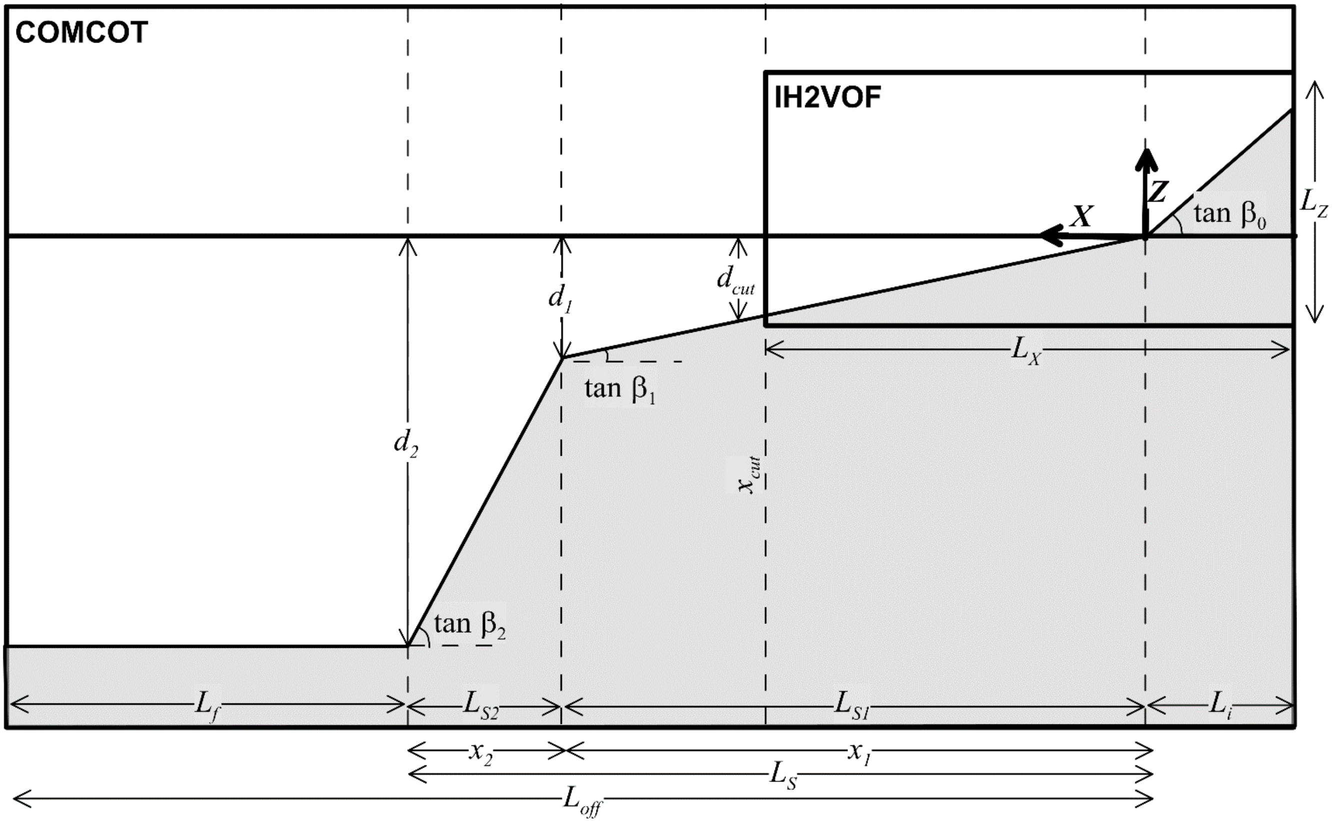

Fig. 4. Numerical flume geometry, including the 5 parameters that define each profile (tan *β1,* tan *β2,* tan *β3, d1* and *d2*) and the general location of *xcut*, where numerical models are coupled

L is determined for each simulation according to the profile parameters (tan β_1, tan β_2, tan β_3, d_1 and d_2), and the tsunami wave length is $\lambda = T \cdot \sqrt{g \cdot h}$, where T is wave period and g is the gravitational acceleration:

$$L = L_i + L_{off} \quad (1)$$

$$L_i = \frac{50}{tan\beta_0} \quad (2)$$

$$L_{off} = L_f + x_2 + +x_1 \quad (3)$$

$$L_f = \left\lceil \frac{1.2 \cdot \lambda}{10 \cdot \Delta x} \right\rceil \cdot \Delta x \quad (4)$$

$$x_2 = \frac{d_1}{tan\beta_1} + \frac{d_2 - d_1}{tan\beta_2} \quad (5)$$

where Δx is the resolution (cell size) of the simulation with the COMCOT numerical model, as described in detail in the next section. In Equation 4, Δx is in both denominator and numerator to round L_f to the order of Δx, by means of "ceiling brackets".

The IH2VOF domain is located in the shallowest part of the profile, with a sufficient area of the inland domain to obtain an accurate measurement of run-up and an area as long as possible for the wave propagation.

The design of the domain of the RANS model (IH2VOF) followed 2 conditions. First, the maximum number of cells in X dimension was set at 5499 (n_x<5499) in order to avoid too long computational times, and the ratio between the dimensions of the cell on each direction must be constant ($r=\Delta x/\Delta z$=constant). In this case, a scale relation of r=5/1 was applied. Although this ratio may lead to a slightly premature breaking of the wave (Jacobsen et al., 2012) but limits the computational times. Therefore, the maximum length covered with RANS model was $L_x=n_x \cdot \Delta x$, what led to IH2VOF grid lengths between 500 m and 25000 m. And second, to control and avoid false wave breaking, the Z dimension of the IH2VOF model grid is discretized in a number of cells, satisfying the expression:

$$\Delta z = \left\lceil \frac{K \cdot H_{COMCOT}}{N_c \cdot 0.05} \right\rceil \cdot 0.05$$

Where K is a safety margin of the model K =1.08 and Δz is defined in the range (0.05< Δz <1). In this case, the wave height was discretized in $Nc = 10$ cells to avoid false breaking. The effect of the ceiling brackets is "rounding to the lowest integer". In addition, IH2VOF grids must follow literature validations (Torres et al (2007, 2009), Lara et al (2011)) to set cell dimensions in order to avoid that the first grid point falls out of the log layer.

2.4 Numerical models coupling

The coupling of the numerical models was focused on accurately locating the border position between the models, x_{cut} (see Fig. 4). This location is optimized in the domain of the IH2VOF model for every tsunami scenario, since that area is the most computationally demanding. Two criteria were followed for this optimization: 1) maximize the area of the IH2VOF domain and 2) simultaneously ensure that the flooding does not exceed the inland end of the IH2VOF domain. In this sense, the number of cells of the IH2VOF model drives the generation of the grid and the position where the models are coupled, x_{cut}, is given then by the value of L_x. In addition, since the flume is non-scaled, it was not possible to cover the whole domain with RANS model due to computational restrictions (i.e., the generation-propagation and inundation areas cannot be calculated without assuming other limitations of scale) but offshore generation and propagation is well solved by NLSWE model, where non-linearities are less relevant in the calculation. In addition, NLSW model do not calculate accurately some physical effects, like undular bores, and due to this, IH2VOF domain is optimized in order to minimize this limitation.

To achieve this optimization, it is necessary to know a rough value of the run-up in advance in order to fit the inland part of the grid L_i to each specific case. In this sense, the more accurate the rough estimate of the run-up is, the fewer inland cells are wasted (without flooding), meaning that the IH2VOF performance is optimized. Clearly, the complete run-up must be fully covered by this model domain, meaning that the vertical length of the onshore grid L_z must be adequate. To determine this horizontal length in advance, each simulation is precalculated with only COMCOT to obtain an approximation of the run-up of the considered tsunami scenario.

The transference of data between models occurs at x_{cut}. IH2VOF requires as input a time series of sea surface deformation and a velocity profile; hence, these data are obtained as an output of bthe COMCOT model. Nevertheless, in most cases, the tsunami wave length λ is considerably longer than the length of the IH2VOF grid L_x ($\lambda > L_x$). Therefore, before the entire wave has passed x_{cut}, the reflected wave has already reached back to that point; as a consequence, the amplitude tsunami wave series from COMCOT used in IH2VOF along x_{cut} would be "contaminated" with the reflected wave.

To avoid this situation, a second simulation with only COMCOT is performed for the considered scenario. In this simulation, the topobathymetric profile is the same, but the slope is set to 0 from x_{cut}, and the right inshore boundary is left open (see Fig. 5). This approach minimizes the influence of the reflection, allowing the input data that COMCOT transfers to IH2VOF to be accurately obtained at the x_{cut} position. Thus, the unaltered wave is used to force the IH2VOF domain, in which simulation reflection on the beach is correctly observed and considered for the run-up calculations.

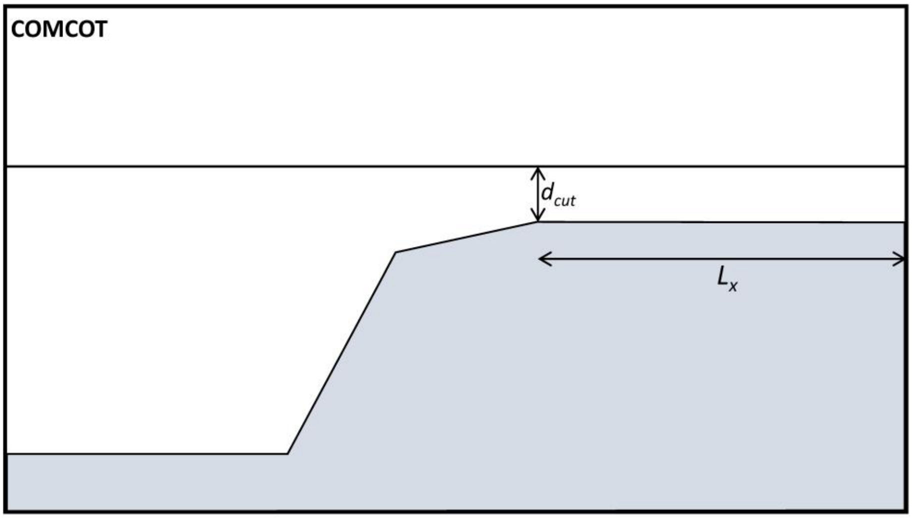

Fig. 5. Numerical flume geometry with a modified profile to avoid the reflection phenomena on the x_{cut} position

To attest the effectiveness of this approach, an example of the wave height propagation of a tsunami wave with *H*=5.6 m for *T*=40 minutes in the numerical flume is shown in Fig. 6. Fig. 6a shows the propagation of the wave height in the unaltered flume with the reflection effects, and Fig. 6b shows the same propagation in the modified flume, in which the reflection effects are minimized. In the plots in Fig. 6, the x-axis is along the length of the flume, the y-axis is the time of the simulation, and the x_{cut} position is marked as a red line. The example wave enters the flume after 10 minutes (600 seconds) of simulation and propagates towards the coast (zero on the x-axis), reaching the x_{cut} position after 30 minutes (1800 s) of simulation. At the x_{cut} position, a reflected wave on the order of 1 m height is reduced by 95%, making it possible to obtain the boundary conditions for the IH2VOF simulation. In some cases the evolution of the wave and the interaction among new tsunami waves could generate effects like standing waves. This effect is not captured by the hybrid model.

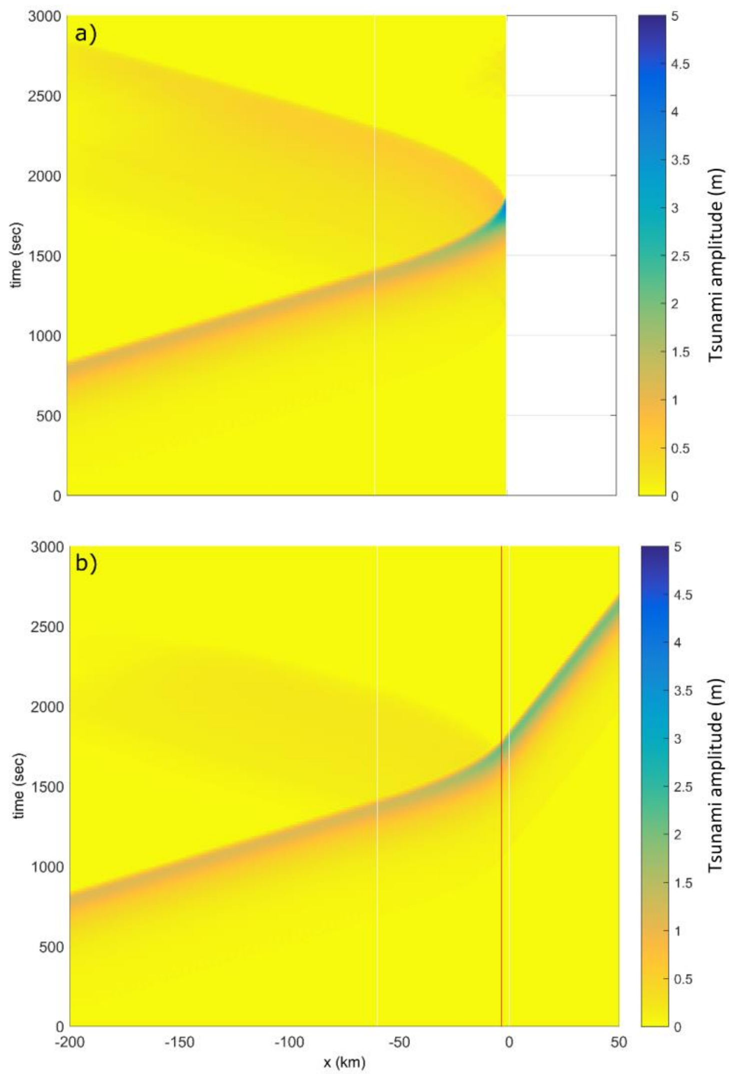

Fig. 6. Propagation of a tsunami wave in the numerical flume on the distance-time plane. x_{cut} position is indicated on the plane with a red line. a) In the initial domain, a reflected wave is observed, aliasing the boundary condition for the IH2VOF domain. b) The modified domain, in which a constant infinite depth is modeled after the x_{cut} position. In this case, the reflection of the wave is eliminated, allowing the boundary conditions for the IH2VOF model to be obtained

Therefore, to sum up, the procedure to simulate the propagation of a tsunami wave in the numerical flume follows the following steps: i) COMCOT domain design based on the profile parameters and tsunami wave; ii) COMCOT simulation to obtain a first estimate of the expected run-up; iii) design of the IH2VOF domain, based on the run-up estimation; iv) calculation of the position of x_{cut}; v) design of the COMCOT domain inland with a modified profile to eliminate the effect of the reflected wave; vi) COMCOT simulation to obtain the boundary conditions (input) for the IH2VOF simulation; vii) IH2VOF simulation and viii) run-up determination in the IH2VOF domain.

The validation of the numerical flume and the coupling of the models was made following several approaches. First, by comparing its results with the results of the physical experiments conducted by **(Synolakis, 1987)** and **(Baldock et al., 2009)**. The scenarios defined on these experiments were calculated using the IH2VOF model in order to assure that the result of the application of the exposed grid conditions (scale relation *r*=5/1) is correct. Fig. 7 shows the run-up obtained in this comparison and how the results of both series of experiments fit adequately with the numerical flume results.

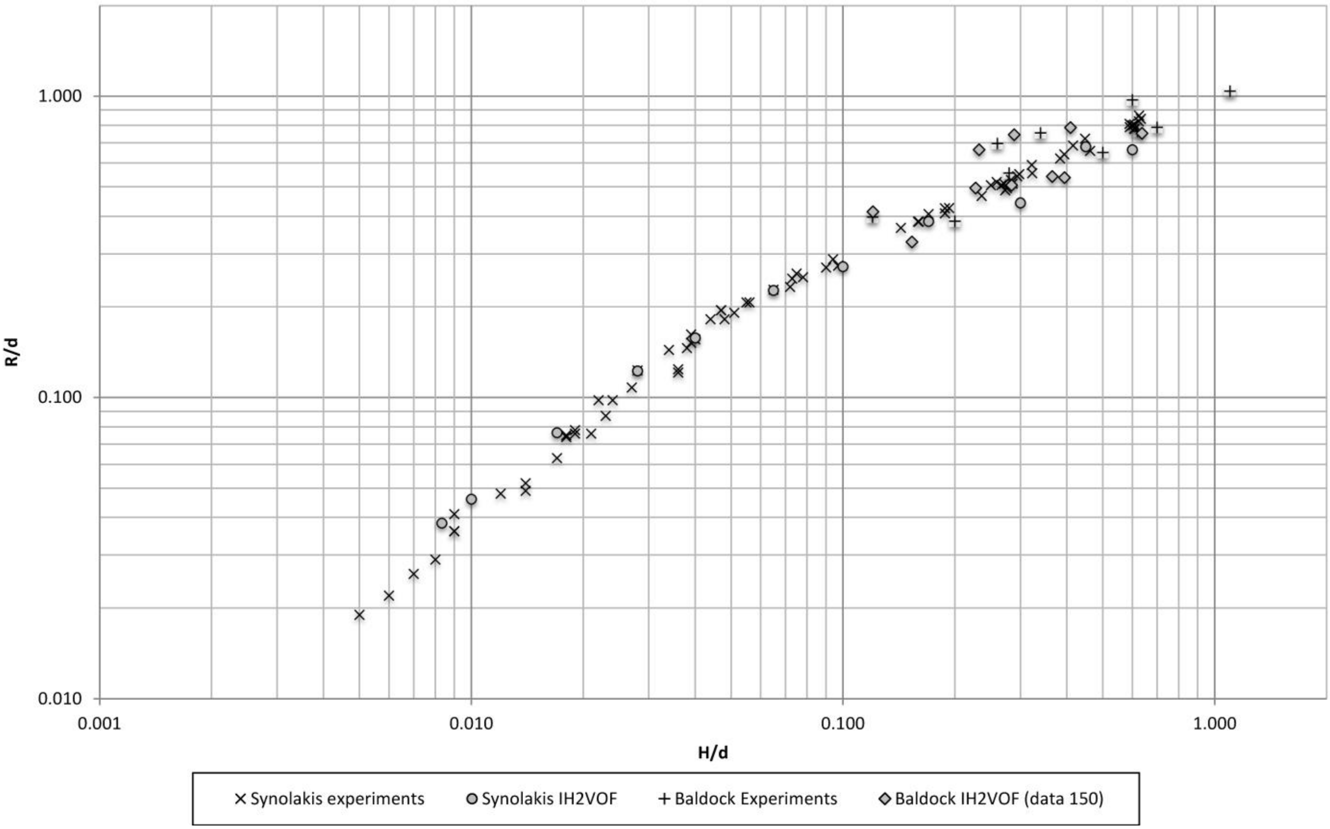

Fig. 7. Validation of the numerical flume by comparing the results of its application with the results of the physical experiments of (Synolakis, 1987) **and** (Baldock et al., 2009)

Additionally, due to the fact that IH2VOF model gives accurate results, the run-up calculated with the numerical flume (COMCOT + IH2VOF) was successfully compared to the result of just applying IH2VOF to the whole geometry for several scenarios. Fig. 8 shows a comparison among 3 propagations of the same scenario: (i) using IH2VOF for the whole domain, (ii) coupling at x_{cut} two IH2VOF domains, and (iii) applying the elaborated numerical flume, coupling COMCOT and IH2VOF at x_{cut}.

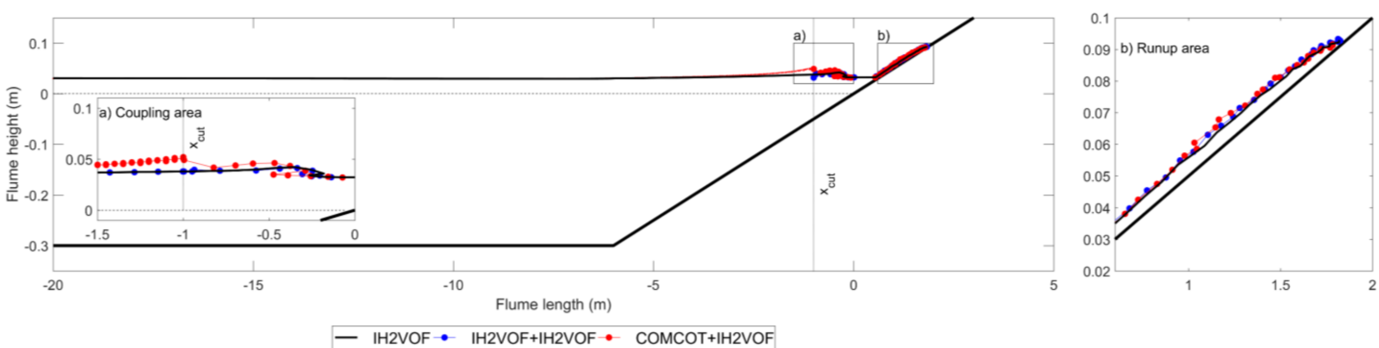

Fig. 8. Comparison among validated IH2VOF model and the numerical flume created within this methodology. Detailed subplots containing the coupling and the run-up areas are depicted in the figure.

To assess the tsunami hazard in a tsunami-prone area, this coupled model can be applied to several profiles all along the studied coastal area. The methodology provides the run-up at each of the profiles, allowing the flooded area to be estimated as an envelope of the run-up limits.

3. Application example: further development of a tsunami run-up database

The presented hybrid model was created with the aim of applying it to generate a tsunami run-up database (TRD) from a combination of bathymetric profiles and tsunami waves. The objective of this database is to create an interpolation space that allows the instant evaluation of the tsunami run-up, without needing to run numerical simulations.

This database contains the run-up of tsunami scenarios that are combinations of parameterized tsunami waves and parameterized bathymetric profiles. These scenarios have been simulated within the described numerical flume.

The following section is focused on explaining the details of the development of the TRD, the selection of the bathymetric profiles and tsunami waves, and the simulations run with the hybrid numerical model. Finally, an interpolation tool, which was developed ad hoc to apply the database to the instantaneous estimation of the run-up, is presented.

3.1 TRD bathymetric profiles

The parameterization of the 50 bathymetric profiles that were selected worldwide (see Fig. 1 and Table 1) were added to the TRD. The 5 parameters of each of these 50 measured profiles were obtained by means of a least-squares fitting method.

To increase the number of cases included in the TRD, more realistic profiles were added as combinations of the 5 parameters. To generate these profiles, the ranges of the values of each parameter over the 50-profile sample set were analyzed, with a focus on identifying trends or rules that characterize their variability. The new profiles follow these trends, avoiding the inclusion of unrealistic combinations of parameters (e.g., $(d_2 - d_1)$ was always larger than 2200 m and x_1 was always shorter than 210 km). By using these realistic combinations of parameters, the TRD was expanded to 5000 profiles.

Finally, from those 5000 profiles, a selection of 49 profiles was made by means of the maximum dissimilarity algorithm (Camus et al., 2011). These 49 profiles assure a maximum variability in the profiles to further develop the TRD. The parameters of the 49 chosen profiles are given in Table A1 of Annex A.

3.2 TRD tsunami wave parameterization

The tsunami waves for the TRD were obtained by means of simulations of realistic scenarios using the COMCOT model, applying a grid size of Δx=500 m and satisfying the CFL condition given by the model ($\frac{C\cdot\Delta t}{\Delta x} < 0.5$, where Δt is the time step of the simulation). Based on these simulations, the tsunami waves were characterized by 2 parameters: tsunami wave height (H) and period (T) at the depth d_2.

To generate the tsunami wave shapes with COMCOT, an infinite horizontal domain with a constant water depth was used. In the analyses of the seven focal mechanism parameters (see 2.2), some simplifications were assumed. First, to generate higher tsunami waves, the three angles were fixed to the combination that provides the maximum tsunami height, i.e., θ=0°, δ=90° and λ=90°. Second, D was defined in Table 2, and a width of $W = (M_0/6.25\mu\gamma)^{1/3}$ is obtained by assuming a rectangular fault with proportion $L/W = 2.5$ and using the M_0 formulation (Table 2). Finally, Kanamori and Anderson (1977) provided a relationship between the seismic moment and earthquake magnitude: $M_w = 2/3 \cdot \log(M_{o)} - 6.07$.

Table 2. Formulations used in the definition of the parameters of the tsunami waves included in the addition to the database

Formulation	Definitions	Source
$D=\gamma L$	$\gamma=6.5\times10^{-5}$	Scholz and Harris (2002)
$M_o=\mu SD$	$S=LW$; $\mu=2.5\times10^{11}$ Aki (1972)	Steketee (1958); Burridge, R. and Knopoff (1967)

Taking these parameters into account, the tsunami waves can be obtained in terms of earthquake magnitude (M_w), focal depth (h_{focal}) and water depth (d). Therefore, the influence of these three parameters on the tsunami wave height and period was explored and depicted in a general scheme in Fig. 9. As it could be intuitively expected, the higher the magnitude of the earthquake is, the higher the tsunami wave height; however, the deeper the focal depth is, the lower the tsunami wave height. On the other hand, regarding the tsunami wave period, the period increases with the earthquake magnitude or focal depth. The water depth in the rupture area affects only the tsunami period, which increases when this depth decreases.

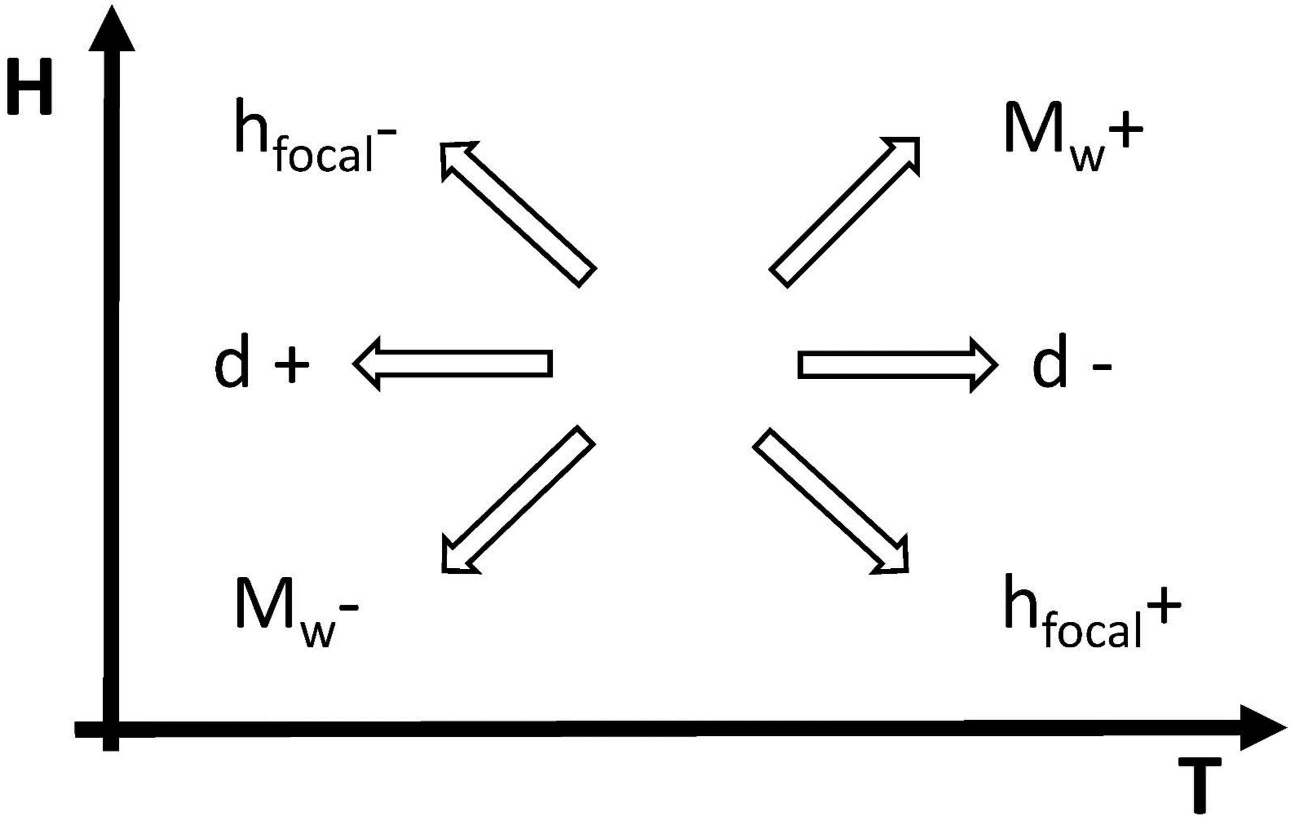

Fig. 9. General scheme of the tsunami wave height (*H*) and period (*T*) behavior in relation to the water depth (*d*) in the generation area and earthquake focal depth (h_{focal}) and magnitude (M_w)

Following this characterization, a set of tsunami waves was selected, covering period values from 5 to 40 minutes and wave height values in the source area (depth d_2) from 0.2 to 2.0 m. In generation areas, tsunami waves are commonly within these ranges (Papadopoulos, 2016). The considered waves are peak or positive waves, meaning that the wave height was considered from the sea level. The tsunami wave heights (from A to K) and periods are given in Table 3. The interpolation is limited to the H and T ranges included in the database. The incorporation of new waves will complement the existing wave database and increase the range of application of the methodology.

Table 3. Tsunami wave height and period at the source area for the current events included in the TRD

Name	Height (m)	Period (mins)
A	1.6	35
B	0.5	35
C	0.5	8

D	0.2	5
E	1.5	15
F	0.5	15
G	1.5	25
H	0.5	25
I	1.0	35
J	1.0	15
K	1.0	25

4. Run-up estimation by interpolation of the TRD

The procedure explained at the end of section 2.4 was followed to calculate the run-up of the combination of the tsunami waves and the 49 topobathymetric profiles. Therefore, the TRD is increased by 539 scenarios, provided by 7 parameters ($tan\beta_0$, $tan\beta_1$, $tan\beta_2$, d_1, d_2, H and T). These simulated scenarios constitute the 7-dimension interpolation domain in which new run-up calculations are carried out. The interpolation procedure and the result of its application are described next. A tool to calculate the run-up by interpolation was developed. This tool allows the simultaneous analysis of the influence of each parameter on the final value of the run-up.

4.1 The interpolation tool (IH-TRUST)

To interpolate the value of the run-up for new scenarios, a numerical tool was programmed. This tool, called *Instituto Hidráulica-Tsunami Run-Up Simulation Tool* (IH-TRUST), processes the profile and wave data to calculate the run-up, and it performs an interpolation of the 7 parameters considered in the TRD. IH-TRUST consists of three modules, or elements (Fig. 10).

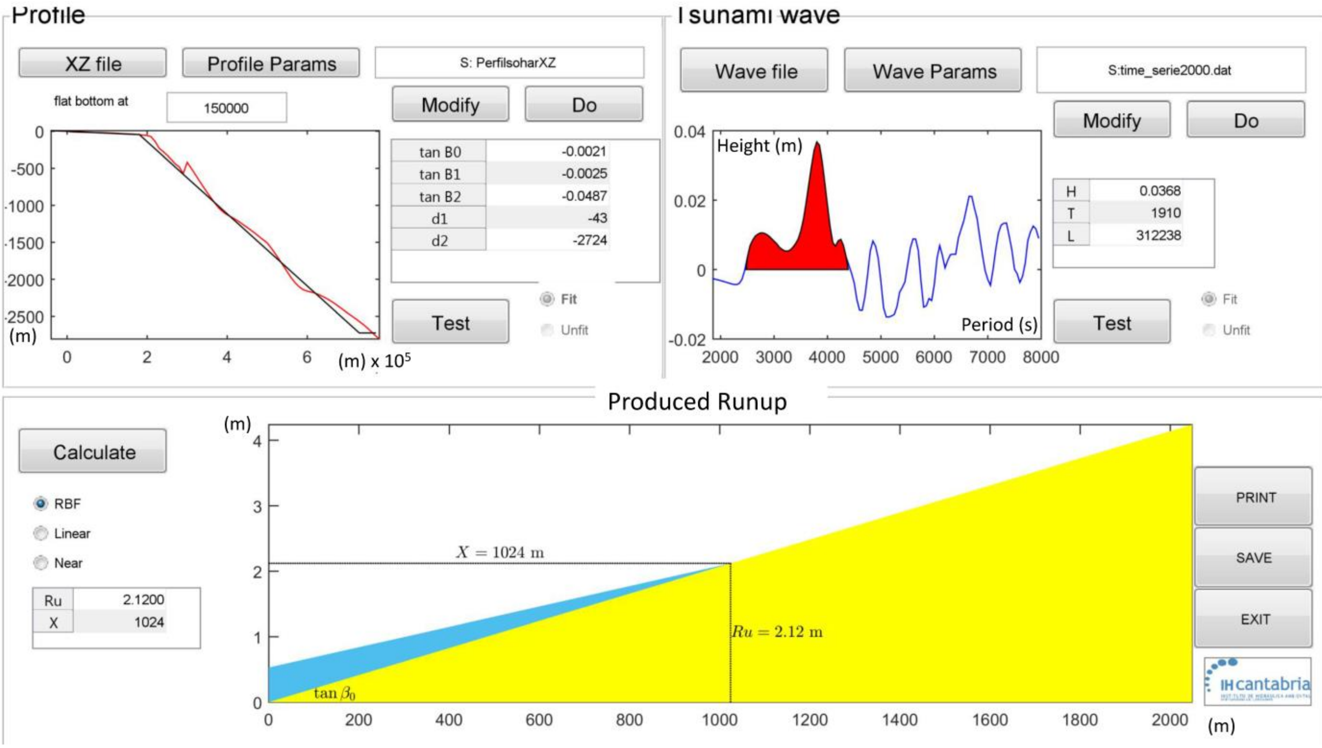

Fig. 10. IH-TRUST interface, showing its 3 elements: the bathymetric profile, the tsunami wave parameterization and the run-up calculation

In the first element, the tool calculates the parameterization of the real topobathymetric profile into 5 parameters: $tan\beta_0$, $tan\beta_1$, $tan\beta_2$, d_1, and d_2. The real profile ideal trace should be parallel to the potential tsunami wave travel. The parameterization is approached by means of a least-squares fitting. An example of the fitting of a profile is shown in Fig. 11, in which the main plot shows the quadratic error in terms of distances from the coast to d_1 (X_1) and to d_2 (X_2), and the star indicates the minimum error, which is consequently the position of the best set of five parameters. The subplot shows the original profile and the parameterized profile. Afterwards, the tool verifies that the parameterized profile is included in the ranges of the parameter values contained in the interpolation space.

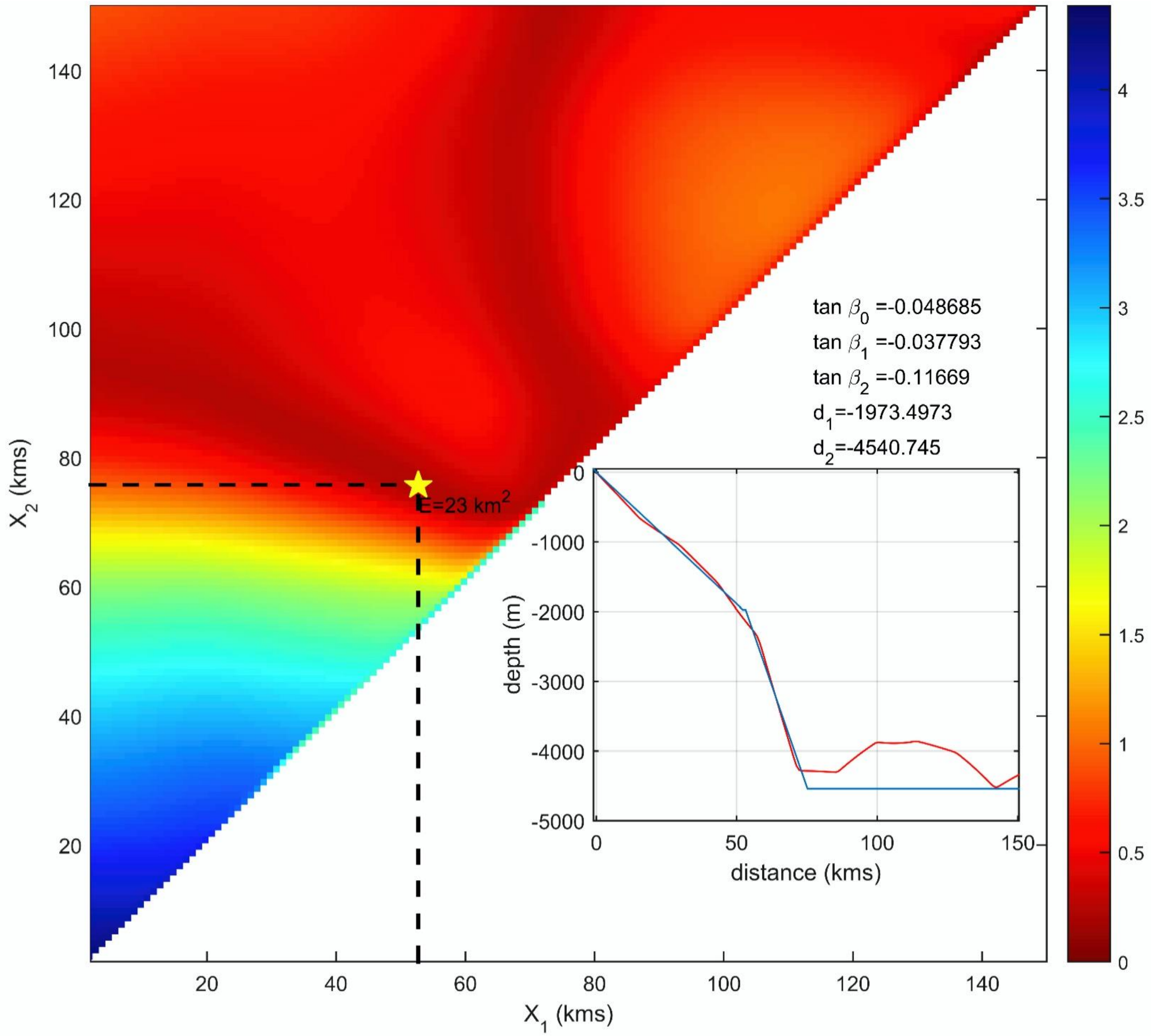

Fig. 11. Parameterization of the bathymetric profiles. The figure maps the E_{rms} values as a function of the distance from the coast to d_1 (X_1) and the distance from the coast to d_2 (X_2) obtained during the process of finding the best parameters for a profile. In the subplot, the original profile and the parameterization are shown

Fig. 12 shows a representation of all the profile domains in black and the introduced profile in red. A set of bars indicates the acceptable values for each parameter, and a star marks the position of each parameter for the new profile.

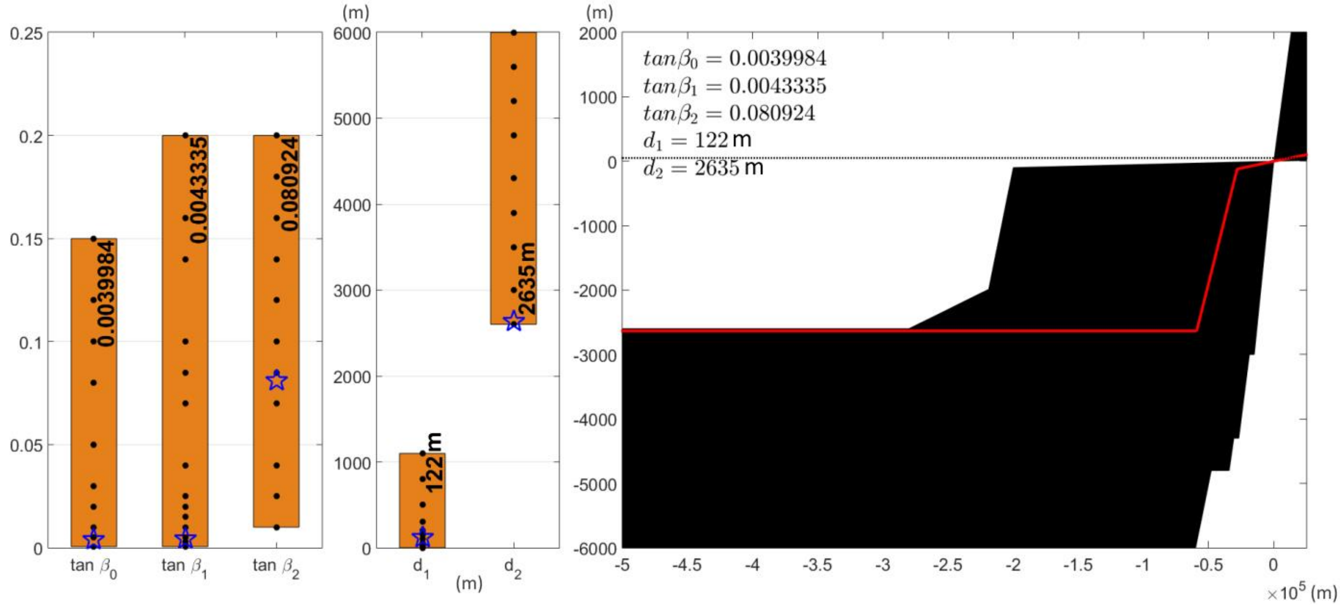

Fig. 12. Fitting of a topobathymetric profile in the TRD. Each parameter value (left) and parameterized profile shape (red) for the profiles are included in the TRD (black)

In the second element, IH-TRUST calculates the values of the amplitude and the period of the tsunami wave to be assessed at depth d_2. The tool reads a time series containing the tsunami shape and calculates H and T. T corresponds to the time between the first two zero crossings for positive heights, and H is the maximum positive amplitude observed within period T, but the tool allows to manually set the height and period within the time series, if desired (Fig. 13). This is especially useful when the wave shape is not standard, the wave has a leading depression or, simply, it is not the largest wave of the series.

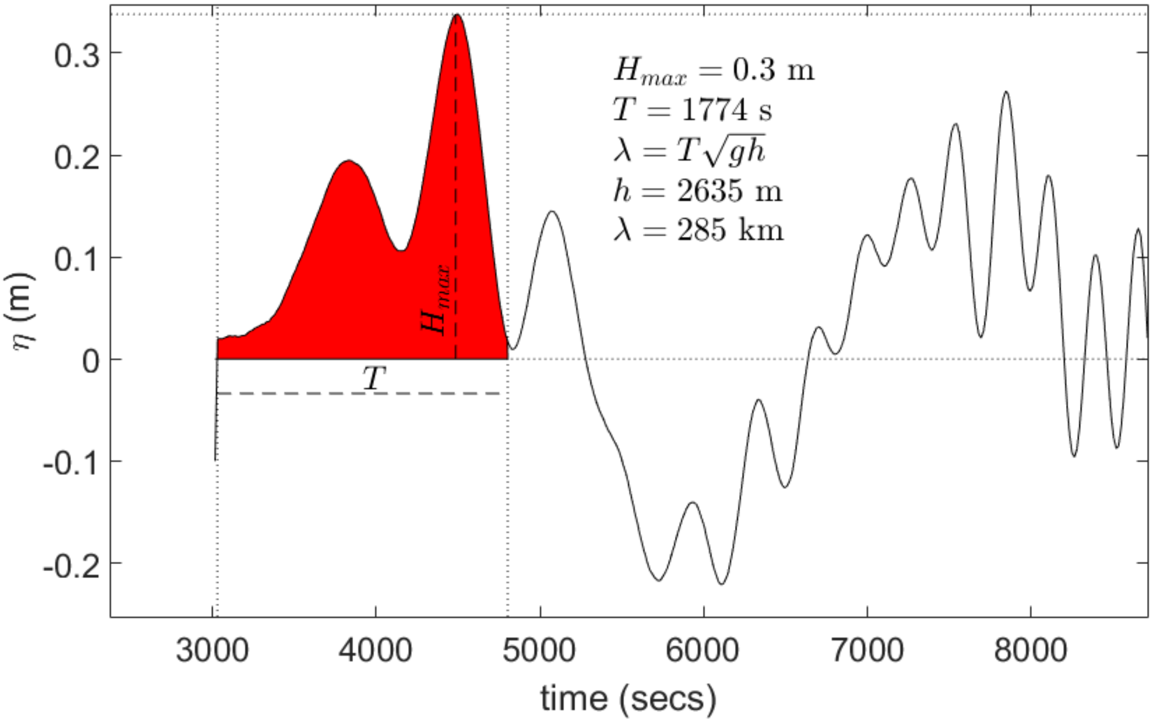

Fig. 13. Tsunami wave profile parameterization in the IH-TRUST tool, including the part of the tsunami time series considered (in red) to calculate the period *T* and the height *H*

After the wave parameters are calculated, IH-TRUST checks if the tsunami wave fits in the interpolation domain of the database. Fig. 14 shows the tsunami waves included on the database, the area where the interpolation is valid and the position of the tsunami wave that is being studied.

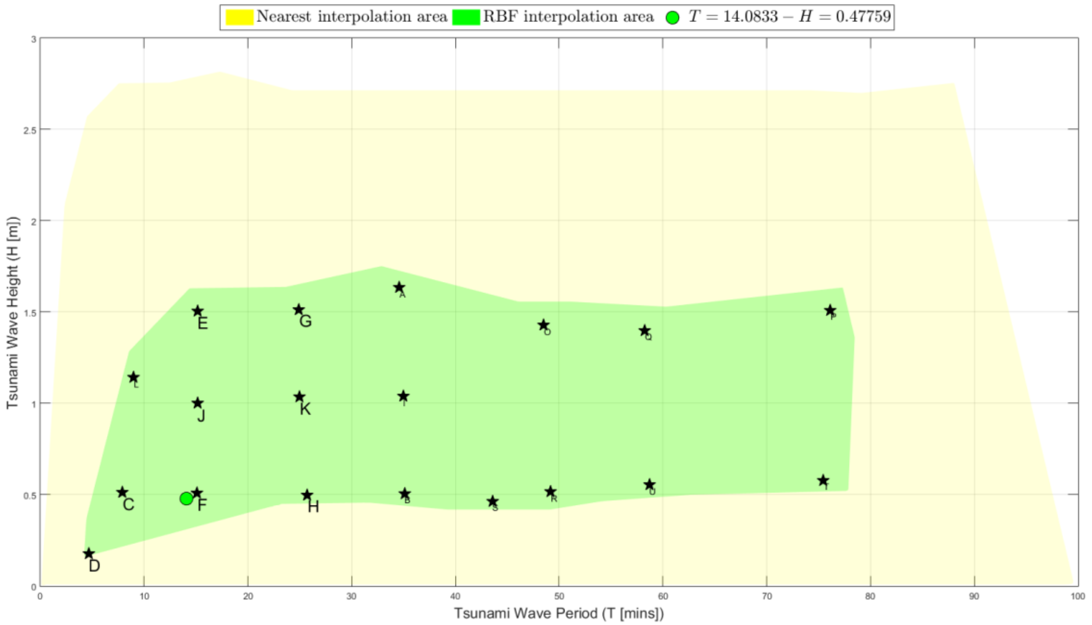

Fig. 14. Tsunami wave height and period cases included in the database. The point corresponding to any new wave should fall in the green shadow in order for it to be able to be interpolated with the generated TRD

Finally, in the third element of IH-TRUST, the results of the calculation of the run-up *Ru* is given based on the profile parameters and the tsunami wave. The interpolation (Fig. 10) is calculated by means of the RBF (Camus et al., 2011) and linear and nearest interpolation methods. In addition, the horizontal flooding distance *X* is calculated using the inland slope. The tool uses an RBF interpolation by default, but the nearest or linear methods are also available, since they are useful to calculate events that plot closer to the boundary of the valid interpolation area.

4.2 Influence of the profile parameters on the tsunami run-up

The TRD and IH-TRUST were used to explore and analyze the influence of each parameter of the profile on the final value of the run-up. This analysis was approached by evaluating scenarios in the TRD. Although it is out of the scope of this paper, to understand the influence of each parameter of the bathymetric profile, several tests were conducted with a mean profile ($tan\beta_{0m}$=0.080, $tan\beta_{1m}$=0.09, $tan\beta_{2m}$=0.110, d_{1m}=500, and d_{2m}=4350) and by varying only one of the 5 parameters that define the profile at a time; additionally, several values of *H* and *T* inside the boundaries of the domain were considered.

For each pair of values of *H* and *T*, 4 of the 5 profile parameters were kept constant, and the run-ups were calculated using IH-TRUST with the TRD by varying the 5th parameter.

The effect of the variation in *Ru/H* as a function of the parameters are shown in Fig. 15 and Fig. 16.

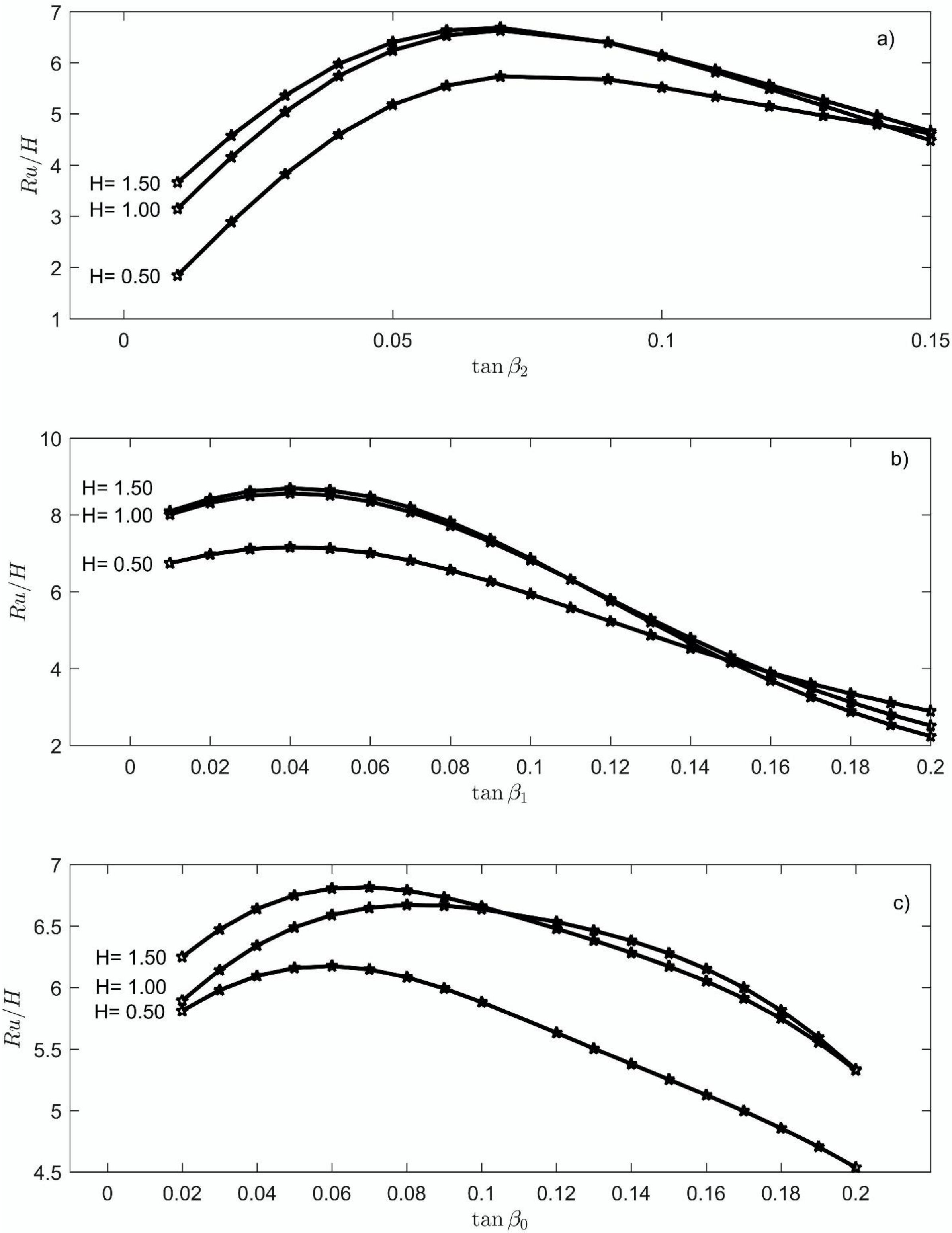

a)
H= 1.50
H= 1.00
H= 0.50
Ru/H
$\tan\beta_2$
b)
H= 1.50
H= 1.00
H= 0.50
Ru/H
$\tan\beta_1$
c)
H= 1.50
H= 1.00
H= 0.50
Ru/H
$\tan\beta_0$

Fig. 15. Maximum run-up (normalized by wave height) as a function of the profile slopes (*tanβ0, tanβ1,* and *tanβ2*) of the parameterized profiles for different wave heights.

The continental slope effect (Fig. 15), parameterized as $tan\beta_2$, produces a maximum *Ru* when $tan\beta_2$ is close to $tan\beta_1$, reproducing a single slope profile. For smaller $tan\beta_2$ values, *Ru* decreases rapidly due to wave shoaling. Low values of $tan\beta_2$ also indicate a large platform with a low slope, where the shoaling increases the wave height and the wave energy diminishes gradually due to bottom friction until wave breaking occurs. Thus, the energy flux that reaches the shore decreases with the run-up height. The profile typology characterized by a low value of *tanβ2* is closer to Synolakis's canonical problem.

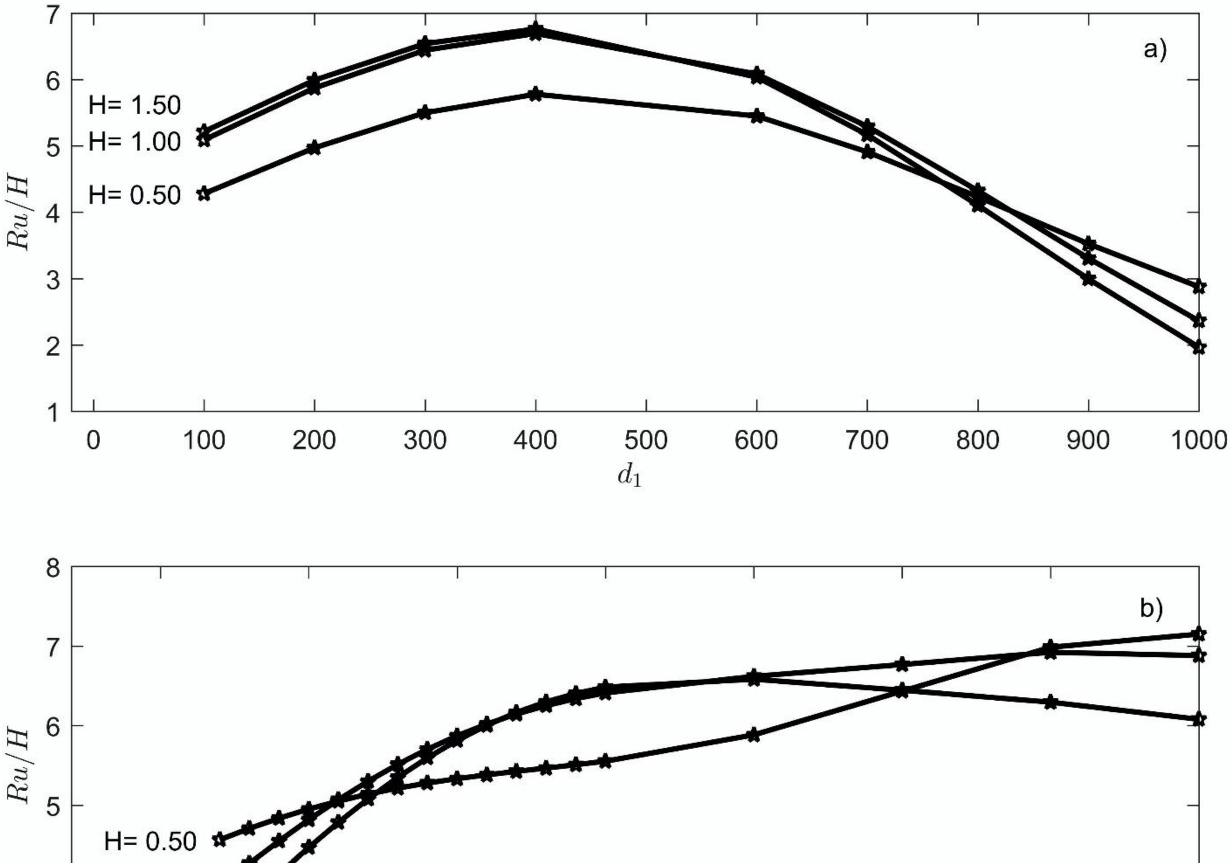

Fig. 16. Maximum run-up heights as a function of the profile slopes (d_1 and d_2) of the parameterized profiles for different wave heights

The higher the $tan\beta_2$ is, the shorter the platform, reducing the energy dissipation and allowing the slopes to have similar $tan\beta_0$ and $tan\beta_1$; this maximizes the run-up height.

Regarding $tan\beta_1$, when d_1 is constant (Fig. 15), the higher $tan\beta_1$ is, the shorter the length of the shelf, reducing tsunami wave shoaling. In this case, the wave steepness increase drastically near the coast and breaks abruptly, triggering a considerable dissipation of energy within a short length; this effect reduces both the energy flux on the coast and the run-up.

Kânoğlu and Synolakis, (1998) shown that in the case of solitary waves the slope closest to the coast controls the run-up processes. In the case of tsunamis, in our geometry, although the influence of $tan\beta_1$ is indeed important, the influence of $tan\beta_2$ must not be neglected.

Finally, the influence of $tan\beta_0$ on the final value of the run-up is less important than those of $tan\beta_1$ and $tan\beta_2$. The run-up decreases as $tan\beta_0$ increases. Due to the effect of gravity, the flow ascends less if greater slopes are present. This aspect is strengthened by the reflection of the energy.

The behavior described above can be summarized on three basic regimes, depiced in Fig. 17. i) The larger run-up for any wave height is found if $tan\beta_1 = tan\beta_2$ (see Fig. 17 b). ii) When $tan\ \beta_1 > tan\ \beta_2$ see Fig. 17 c, the bigger the difference between slopes, the smaller the run-up run-up mainly because the increase of dissipation; and iii) when $tan\ \beta_1 < tan\ \beta_2$, see Fig. 17 d, the run-up is also smaller, but in this case it is due to the effect of increasing reflection.

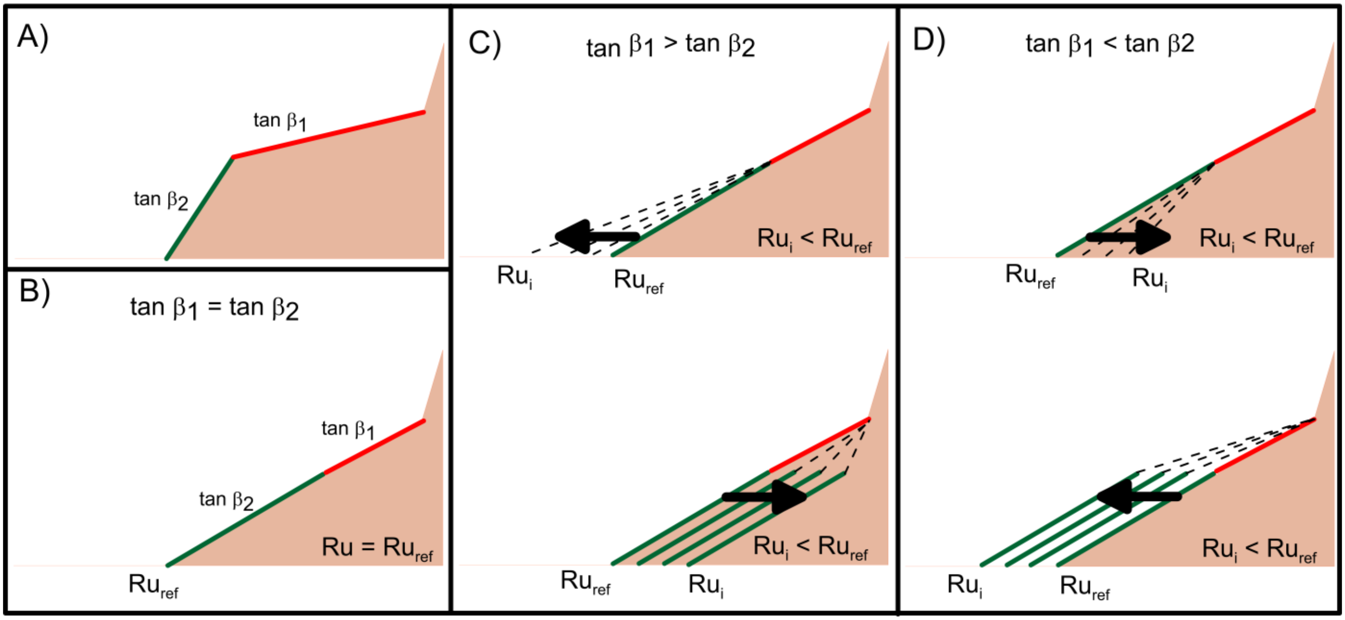

Fig. 17. Influence of the variation of the *tanβ₁* and *tanβ₂* on the run-up. A) shows a scheme of the profile where segment of *tanβ₂* is marked as green and *tanβ₁* as red. B) shows the situation where *tanβ₁* = *tanβ₂*. C) depicts the situations where *tanβ₁* is larger than *tanβ₂*. And, finally, D) shows the situations where *tanβ₁* is smaller than *tanβ₂*.

The influence of depths d_1 and d_2 is shown in Fig. 16. For deeper continental shelf depths d_1, the shelf is wider and, consequently, the bottom friction affects the wave over a longer profile, creating a run-up smaller. For a constant $tan\beta_1$, lower values of d_1 represent a shorter continental shelf, and abrupt and dissipating wave breaking. Moderate values of d_1 are characterized by a gradual tsunami wave shoaling, during which the bottom friction allows a maximum run-up. From that critical point, higher values of d_1 mean a longer continental shelf, generating a larger frictional area, reducing the energy flux that reaches the shore and consequently diminishing the run-up.

In Fig. 16b, it can be observed how the run-up increases almost linearly with d_2. The effect of d_2 in the run-up is similar to the effect of $tan\beta_2$. The shallower d_2 is, the greater the shoaling and the higher the wave. The wave energy diminishes gradually due to bottom friction until wave breaking, which depends on the tsunami wave height. In addition, it was found that although the variations in wave height produce different *Ru/H* values for the same profile, the influence of the variation in the wave period is negligible. Therefore, different wave heights but not different periods are shown in Fig. 15 and Fig. 16.

Finally, these results highlight the importance of using an accurate geometry to define the run-up. The influence of d_2 and $tan\beta_2$ in the final run-up estimation is considerable, and the use of complete profiles, from the generation area to the coast, is necessary but not considered in traditional approaches and simplifications.

5. Validation of the methodology with numerical test results and observational data

The methodology presented here aims to calculate the tsunami run-up in coastal areas. This calculation can be applied to study the run-up of historic events but also to calculate the run-up of potential scenarios, which are the primary focus. These potential cases are used to evaluate tsunami hazard and the flooded area when a tsunami occurs. As mentioned in the introduction, run-up is commonly assessed by means of high resolution data.

Therefore, to validate this methodology/tool, the results of its application have been compared with both high-resolution numerical simulations of potential events and historical tsunami run-up scenarios. It is important to highlight that the presented tool allows to estimate tsunami run-up when these HR data are not available or accessible, what is a common situation.

The results of these comparisons are detailed in the following subsection, which is focused on describing the strengths and limitations of the methodology for each case.

5.1 Validation with numerical model simulations

This validation was carried out as follows: first, a topobathymetric profile of the study area was obtained using the GEBCO database. On that profile, a point was selected offshore, and the time series of the tsunami was extracted at that point from the COMCOT numerical simulation of the event. Using the topobathymetric profile and the time series as input for the IH-TRUST tool, the run-up was interpolated by using the created database. The interpolated run-up was then compared to the run-up obtained by using the high-resolution numerical simulation of the potential scenario.

Three numerically simulated scenarios with high resolutions have been selected for the validation. All these scenarios are from real projects, studies and published papers that were focused on analyzing and assessing the tsunami hazard in coastal areas worldwide and characterizing the potential flooded areas due to tsunami events in the selected zones. These simulations used high-resolution topographic and bathymetric data to construct grids with 30 m cells.

5.1.1 Tsunami scenario in Trujillo, Peru

The results of the application of the methodology were compared to the results of a high-resolution numerical simulation of a magnitude 8.5 event in the subduction zone located along the coast of Trujillo, a municipality in northern Peru. This synthetic scenario represents the event that occurred in this zone in 1619 and is part of the study *Probabilistic evaluation of the hazard and vulnerability under natural disasters in the metropolitan area of Trujillo*, funded by the Inter-American Development Bank (IHCantabria, 2013). The numerical simulation used a 30-m-resolution grid to accurately calculate the flooded area for a tsunami wave height and period of approximately 1.5 m and 400 s at a depth of 3000 m.

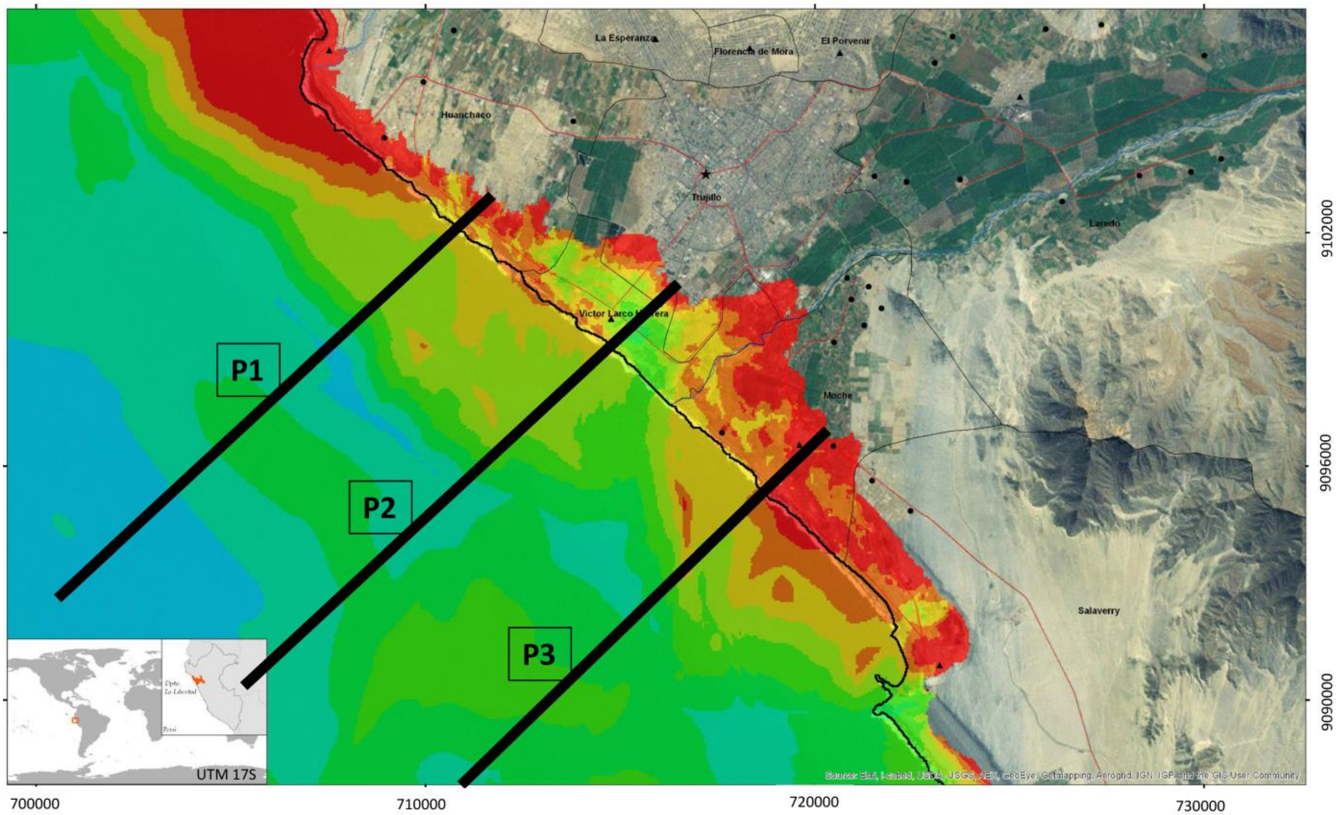

Fig. 18. Flooded area in the municipality of Trujillo in Peru, due to a tsunami triggered by an 8.5 magnitude earthquake, including 3 selected profiles with the run-up obtained by using the numerical model. The coordinates of the exact locations where the run-up was estimated are provided in Table 4

In Fig. 18, the flooded area map of Trujillo, as well as the selected profiles, are shown. In the study, the numerically calculated run-ups at those profiles (Fig. 19) were 8.9, 10.6 and 12.8 m. The corresponding values for the run-up obtained by interpolating the TRD with the IH-TRUST tool were 8.8, 10.5 and 11.6 m (see Table 4). Compared to the results of the numerical simulation, these 3 values from the 3 zones of the study area provide a good approximation of the tsunami flooding.

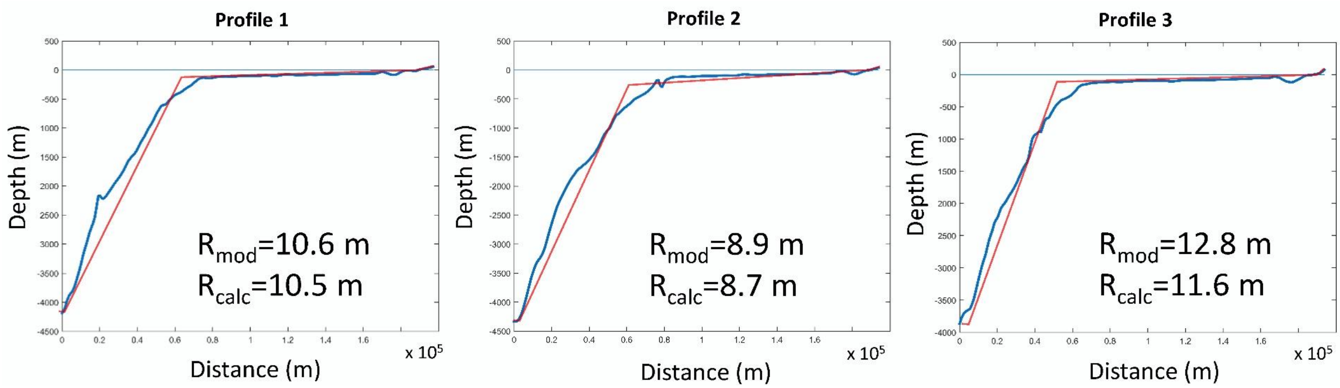

Fig. 19. Topobathymetric profiles selected in Trujillo, Peru to validate the methodology. The topobathymetric profile (blue) and the parameterized profile (red) are compared

5.1.2 Tsunami scenario in La Libertad, El Salvador

Following the same procedure, a validation case was addressed in El Salvador. The event is a potential scenario of an earthquake of magnitude 8.1 along the El Salvador thrust, which is in the subduction zone along the El Salvador coast. The study area is the flat area of La Libertad, on the western side of this Central American country. This high-resolution numerical simulation is part of the project *Tsunami Risk Assessment in El Salvador*, financed by AECID (Spanish Agency for International Cooperation and Development) during the period 2009–2012 (Álvarez-Gómez et al., 2013). The resolution of the numerical simulation was 30 m, and the grid that was built for the propagation and inundation calculations used data from local bathymetric campaigns and high-resolution topographic studies. The tsunami wave height and period at a depth of 3000 m were approximately 0.9 m and 700 s.

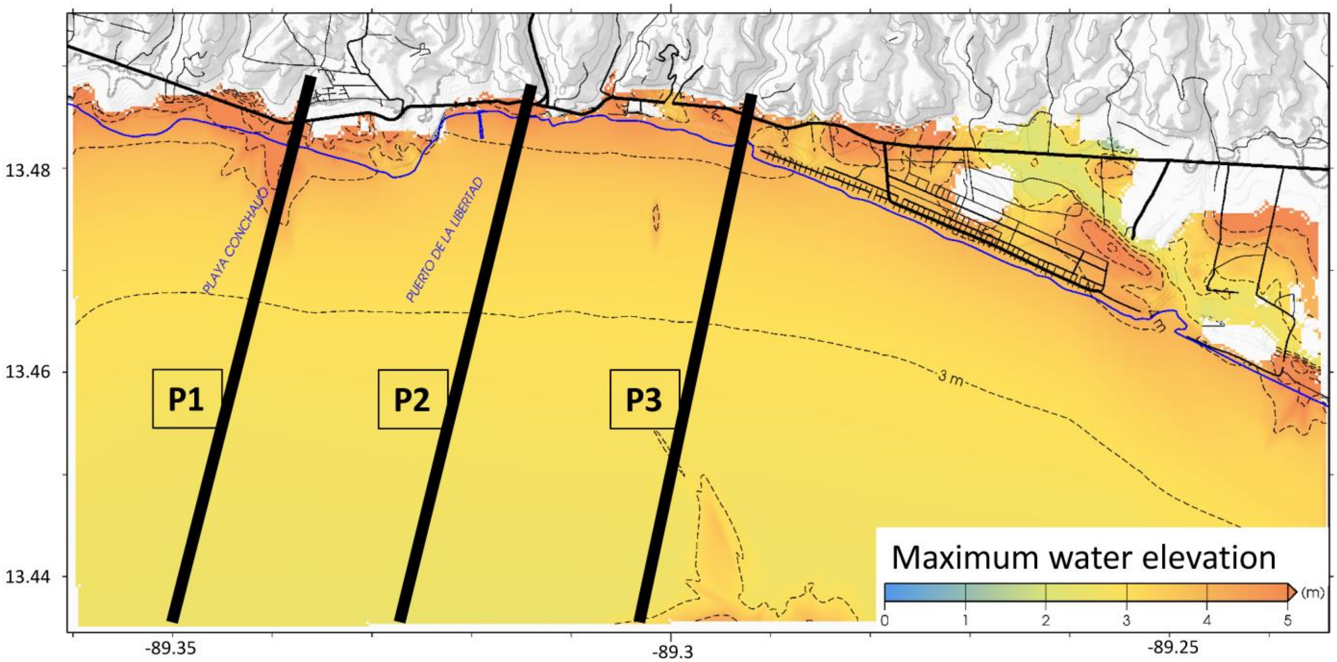

Fig. 20. Flooded area in the municipality of La Libertad in El Salvador, due to an 8.1 magnitude event with epicenter along the coast of this Central American country. The exact locations where the run-up was estimated are provided in Table 4

In Fig. 20, the flooding map that was part of this project is shown, and in the same figure, the selected profiles have been superimposed. In this simulation, the run-ups obtained at the three profiles in Fig. 20 were 5.2, 5.5, and 6.3 m. The corresponding run-ups obtained by interpolating the TRD with the IH-TRUST tool were 6.2, 6.1 and 7 m.

5.1.3 Tsunami scenario in Muscat, Oman

As part of the Multi Hazard Risk Assessment System of Oman (Aniel-Quiroga et al., 2015), more than 3000 potential tsunami events were numerically modeled. A selection of these events were selected to assess the tsunami hazard for some specific municipalities in Oman by means of high-resolution numerical simulations of the generation, propagation and inundation processes, with a 30 m grid. One of these cases was an extreme event of magnitude 9.0 with epicenter in the Makran Subduction Zone (MSZ). For the capital city area, Muscat, the resultant flooding map is shown in Fig. 21; the profiles that were selected for the validation are superimposed on this map. The tsunami wave height and period offshore were approximately 2 m and 2300 s. In these cases, the measured run-ups at each profile were 6.2, 8.7, and 7.7 m. The corresponding run-ups calculated with the new database were 6.3, 8.5, and 7.8 m.

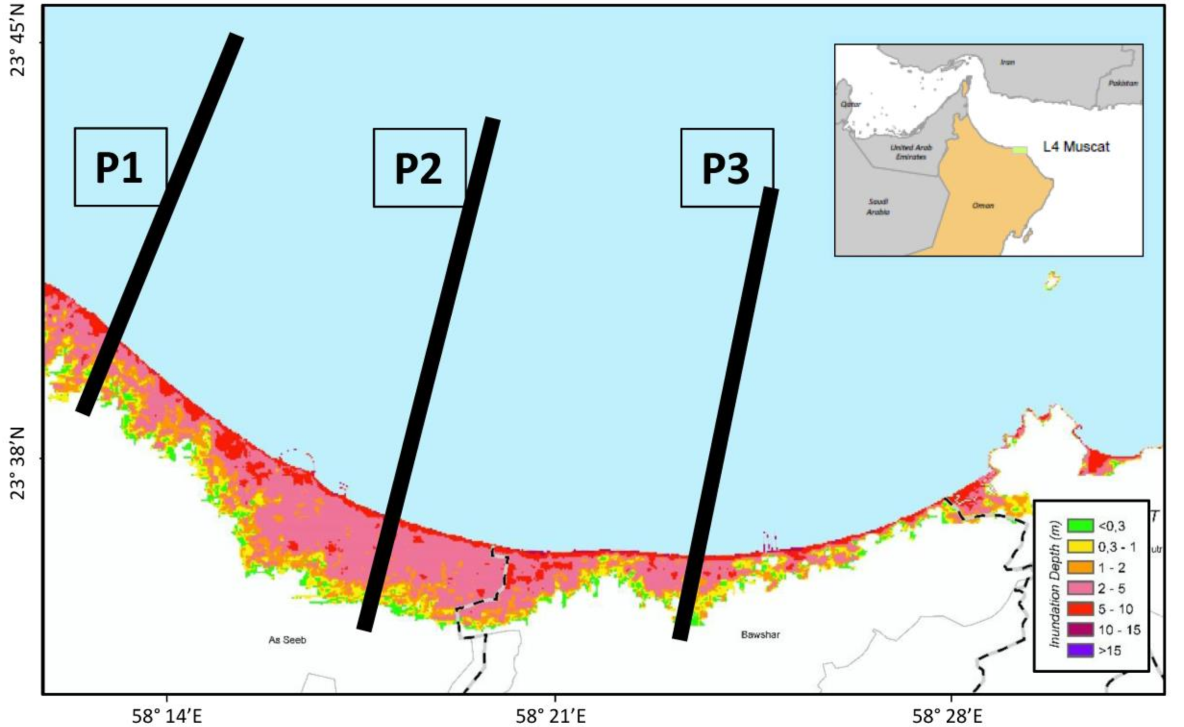

Fig. 21. Flooded area in the municipality of Muscat, capital city of Oman, due to a 9.0 magnitude event with epicenter in the Makran Subduction zone. The extracted locations where run-up was estimated and the run-up values, both modeled and estimated with the IH-TRUST tool, are provided in Table 4.

Table 4 summarizes the results obtained for the validation with the high-resolution simulations in the three scenarios. The run-up values, both those calculated with the numerical model and those estimated with the proposed database and detailed methodology described above, have a similar magnitude; in some cases, the result is accurate enough to rely on the results of the presented methodology. In addition, in Table 4, the estimated run-up is also compared to the result of applying 2 empirical run-up formulae. First, the Synolakis formula, that although it was created for the run-up of Solitary Waves it has been widely applied in the past for tsunamis, and second, Madsen and Schäffer expression for single waves (Madsen and Schäffer, 2010). In the application of this expressions an averaged slope was considered.

Table 4. Tsunamis scenarios included in the validation process of the database and tool. The numerical model column includes the run-up obtained with the high-resolution numerical simulations and can be compared to the estimations from the application of the IH-TRUST and formulae of Synolakis (Synolakis, 1987) and Madsen and Schäffer (2010)

	Coordinates of the run-up point			Run-up			
Place	lon	lat	z	From model	From Method	From Synolakis	From Madsen
	-80.035	-9.07239	2000	10.64	10.54	8.2	18.0

Trujillo (Perú)	-80.23769	-9.02625	2000	8.9	8.79	8.1	12.4
	-80.184535	-9.1122838	2000	12.8	11.64	9.9	18.5
Muscat (Oman)	58.252483	24.026722	1400	6.2	6.35	8.2	7.5
	58.3063	24.01996	1300	8.7	8.57	8.8	7.6
	58.446381	24.025935	1500	7.7	7.87	10.4	6.4
La Libertad (ElSalvador)	89.63894	12.78405	3000	5.28	6.2	6.9	10.2
	-89.595559	12.7768479	3000	5.5	6.13	7.0	10.3
	-89.575252	12.776232	3000	6.3	7.04	6.9	10.3

Fig. 22 shows this comparison in a plot, in which the fitting between the modeled and calculated run-up values is noted. In addition, the new methodology is better than the result of the Synolakis and Madsen and Schäffer formulae, which generally overestimates the run-up.

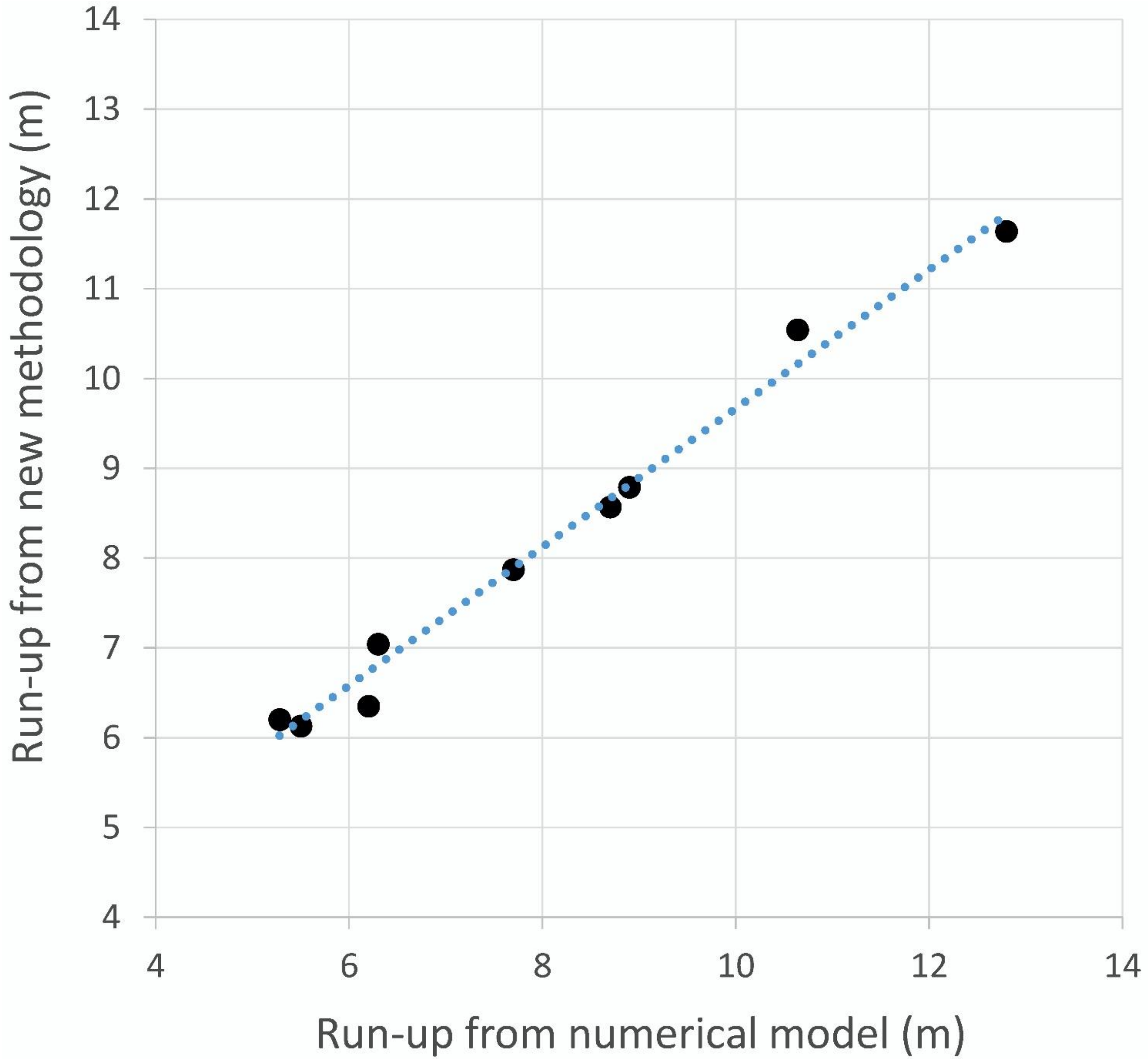

Fig. 22. Plot of the numerically modeled run-up against the calculated run-up values for the validation cases.

5.2 Validation with data recorded during field campaigns after real events

The low frequency of major tsunamis are invaluable to the field campaigns that are carried out immediately after a tsunami event occurs. These field campaigns allow the evaluation of the developed strategies of risk reduction and the creation of new, more accurate strategies. From a pragmatic point of view, the data collected during these campaigns allow scientists and engineers to validate or calibrate numerical models and methodologies. In this case, this type of validation has been addressed using the available field data of the events in Japan (2011) and Chile (2010 and 1960). The bathymetric profiles used in the validation have been constructed using GEBCO. The tsunami wave time series have been obtained from the data available from DART buoys (Meinig et al., 2005) or numerical simulations of accurate sources; this process is explained in detail later in the paper. The results of the application of the methodology have been compared to observational data recordings and field survey papers.

5.2.1 2011 tsunami on the coast of Japan affecting the Pacific basin

On the 11th of March, 2011, a 9.0 earthquake, which had an epicenter close to the coast of Japan, triggered a tsunami that reached the coast of Japan within one hour. This tsunami wave propagated across the Pacific Ocean, reaching the U.S. West Coast in 10 hours and the coast of Chile in 21 hours.

The tsunami wave time series used for this validation have been obtained from the data available from DART buoys (Meinig et al., 2005). The results were compared with the observed run-up (National Geophysical Data Center NOAA).

It is essential to highlight that the application of the new run-up estimation methodology is restricted to the profiles and wave shapes whose parameters fall inside the ranges covered by the database (see Table 1). Therefore, the use of the methodology is limited to these cases. An example of non-applicability occurs when the tsunami height and period are obtained (d_2) in a shallow area of the ocean or when the generation zone is too close to the study area and a complete time series of the tsunami wave cannot be properly recorded at an adequate depth.

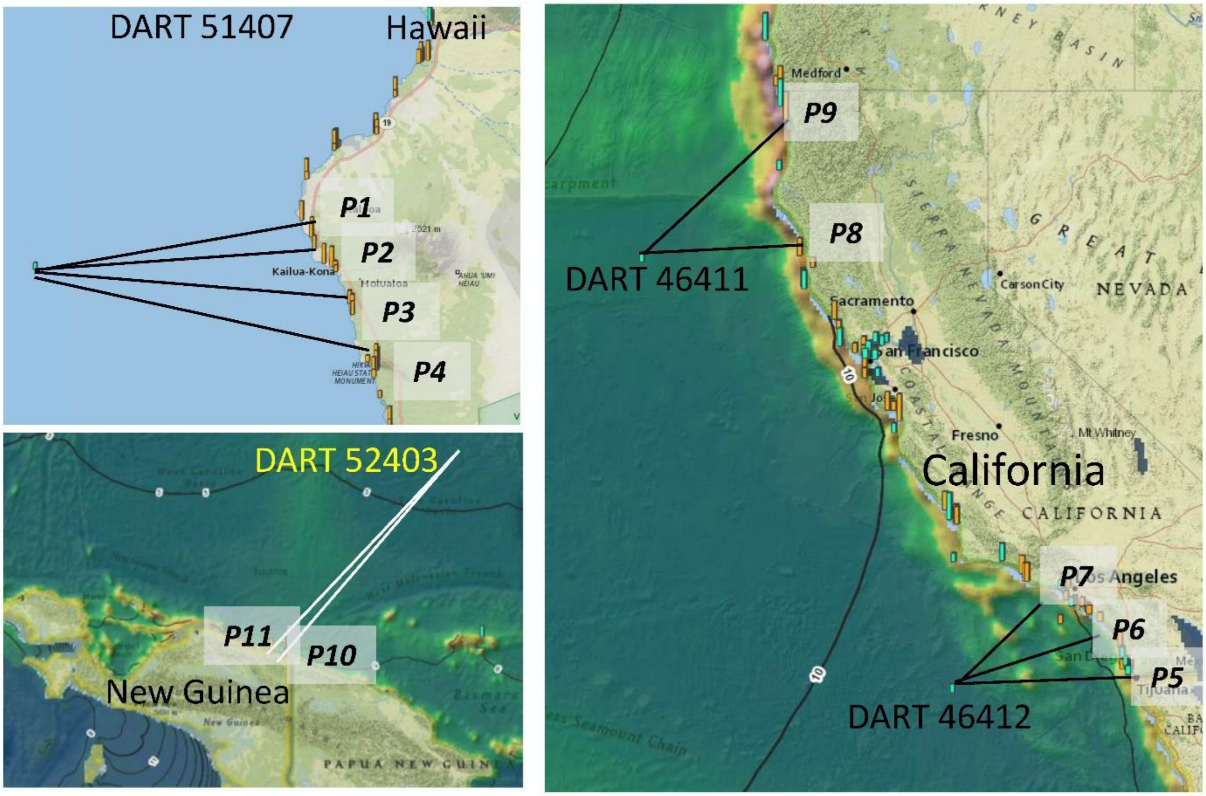

Fig. 23. Validation with DART buoy time series. 4 DART buoys were used, and their data were applied to several bathymetric profiles to validate the methodology. The locations of the points where the run-up was estimated are included in Table 5

In the case of the Japan 2011 event, due to the proximity of the coast, it was not possible to obtain a complete time series between the epicenter and Japan, and the validation has been carried out in other areas of the Pacific Ocean, using four DART buoy records (near Hawaii, California, and Papua-New Guinea). The names and locations of the DART buoys used are given in Table 5. This table also includes the names and locations where the run-up was estimated with the data of each DART buoy, the run-up value recorded in the field surveys at those locations, and the estimated value of the run-up, both by using the new methodology and by applying the Synolakis formula (calculating the tsunami wave height at a depth of 10 m using Green's law) and Madsen and Schäffer formula. The buoy locations are also included in Fig. 23.

Table 5. Validation with DART buoy time series of the Japan 2011 event. 4 DART buoy datasets were used on several bathymetric profiles to validate the methodology. Location names correspond to those given by the National Geophysical Data Center (NOAA). Synolakis run-up was estimated by applying the so-called Green's Law to the time series of the DART buoys to obtain the tsunami height near the coast.

DART Buoy							Run-up (m)			
#	**LON**	**LAT**	**DEPTH (m)**	**LOCATION**	**LON**	**LAT**	**SURVEY**	**Synolakis + Green**	**IH-TRUST**	**Madsen And Schäffer**
51407	-156.5	19.620	4771	**P1 Wawalolo**	-156.05	19.71	2.4	3.8	2.0	1.67
				P2 OldAirport	-156.01	19.64	3.1	3.8	2.0	1.69
Hawaii				**P3 Kahaloo**	-155.97	19.58	2.0	3.8	2.4	1.72
				P4 Keel	-155.93	19.46	3.0	3.8	2.8	.174
46412	-120.7	32.250	3776	**P6 Ocean Beach**	-117.26	32.74	1.0	1.9	1.5	1.07
California				**P7 Marina del Rey**	-118.45	33.98	1.0	1.9	1.9	1.13
				P5 Channel Islands	-119.22	34.15	1.2	1.9	1.4	1.21
46411	-127.0	39.340	4319	**P9 Jenner River**	-123.1	38.43	1.0	2.7	1.1	1.75
California				**P8 Dolphin isle**	-123.8	39.43	1.0	2.7	1.3	1.98
52403	145.52	4.020	4474	**P10 Holtekamp**	140.779	-2.627	2.0	2.3	1.7	3.64
Papua-New Guinea				**P11 Pelabuham**	140.368	-2.461	1.3	2.3	1.4	3.67

As it can be inferred from the application of the methodology, the run-up estimated values are on the same order of magnitude as the recorded inundation; generally, the results are accurate, and differences are normally lower than 20%. These results are also closer to the observed run-ups than those obtained by applying Synolakis and Madsen and Schäffer formulae, which often overestimates the run-up.

5.2.2 Chilean coast tsunamis (2010 and 1960)

When no real record is available to determine the offshore wave shape (DART buoys), the main issue is the correct definition of the source to compute an accurate numerical simulation. Although there is no shortage of uncertainties in the determination of the source, the tsunami initial surface deformation models that have been developed are accurate (Barrientos and Ward, 1990). As an alternative validation approach, two of these models have been used to validate the new run-up estimation methodology with the events that occurred in Chile in 2010 and 1960.

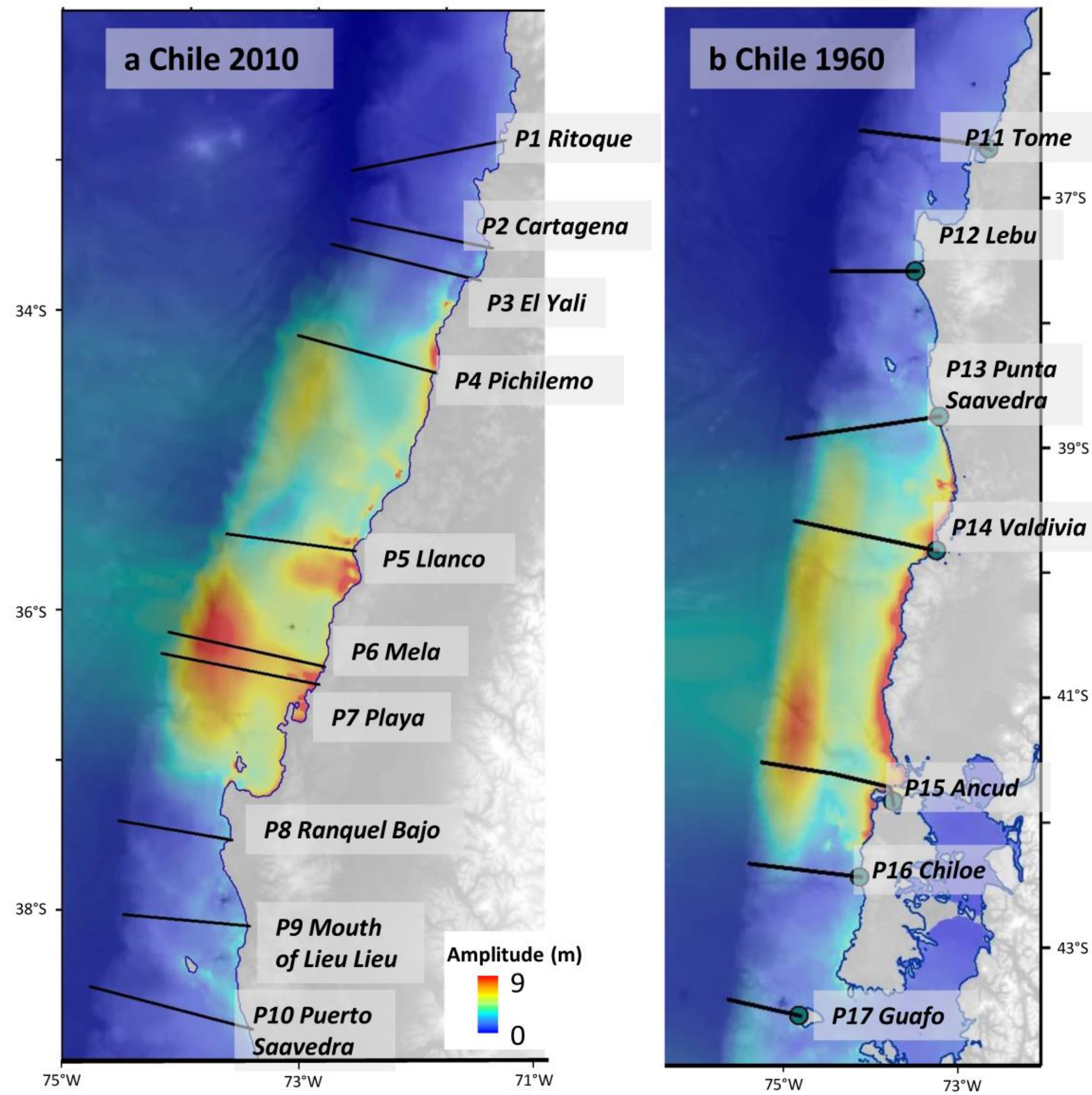

Fig. 24. Profiles and locations used in the validation of the new methodology by using the run-up recorded after the tsunami events of 2010 (a) and 1960 (b) in Chile. The locations of the points where the run-up was estimated are included in Table 6

On the 27th of February, 2010, an 8.8 magnitude earthquake with epicenter on the coast of Chile triggered a tsunami that reached the Chilean coast in less than 30 minutes. In the Bio-Bio region, the run-up was recorded at several locations (Fritz et al., 2011). To apply this methodology, first, a rough numerical simulation of the generated tsunami was addressed. This simulation used the source definition by (Shao et al., 2010) and gridded the GEBCO data with 700 m cells (see Fig. 24). From this simulation, the profiles and wave amplitude time series in the generation area were obtained. The tsunami wave height and period recorded at each location and the result of the interpolation from the further improved database for each corresponding profile are given in Table 6.

The optimal application of the run-up estimation methodology is achieved at the locations sufficiently far from the source, as explained in the previous subsection. The result at these points (1, 2, 3, 8, 9 and 10) have the same order of magnitude of the recorded run-up from Fritz's survey. In the locations in front of the source, the initial deformation of the water surface did not allow a complete time series to be obtained to estimate the tsunami wave height and run-up.

Regarding the 1960 earthquake and tsunami in Chile (Lomnitz, 2004) (Fig. 24), this earthquake is considered the greatest earthquake ever recorded, and the numerical simulation computed for the validation used the source by Barrientos and Ward (1990). The run-up data for the validation was obtained from the NOAA global historic tsunami database. In this case, the data are mainly from eyewitness testimony.

In Table 6, the results of the application of the methodology at 7 locations and the recorded run-up are given. In this case, the tsunami wave height at 3 of the locations (P13, P14, and P15), was such that the profiles were not within the database application ranges. The other 4 locations provided results that are on the same order of magnitude as the observed run-up.

In the application of the new methodology to the Chile events, the tsunami wave height used for the interpolation came from a numerical simulation, and the results were compared to real run-up records. Although the validation inherits the uncertainties of the source, the results are sufficiently accurate, taking into account the limitations explained above.

Table 6. Validation of the methodology with the results of numerical simulations of realistic sources of the 1960 and 2010events on the coast of Chile. Fritz et al. (2011) **survey results were used to validate the results from the new methodology for the Chile 2010 event. NOAA´s National Geophysical Data Center data were used to carry out the comparison with the 1960 event**

					Run-up (m)	
	PROFILE	**LOCATION**	**LON**	**LAT**	**SURVEY**	**IH-TRUST**
2010 event	P1	**Ritoque**	-71.528	-32.826	3.4	1.39
	P2	**Cartagena**	-71.602	-33.542	4	1.93
	P3	**El Yali**	-71.717	-33.751	2.1	3.47
	P4	**Pichilemo**	-72.005	-34.384	5	N/A
	P5	**Llanco**	-72.623	-35.584	11.4	N/A
	P6	**Mela**	-72.852	-36.36	3.1	N/A
	P7	**Playa**	-72.911	-36.478	6.6	N/A
	P8	**Ranquil Bajo**	-73.596	-37.526	5.7	2.2
	P9	**Mouth of Lieu Lieu**	-73.449	-38.097	2.3	2.2

	P10	**Puerto Saavedra**	-73.701	-38.783	2.5	2.3
1960 event	P11	**Tome**	-72.962	-36.619	2.5	3.4
	P12	**Lebu**	-73.674	-37.608	4	4.6
	P13	**Punta Saavedra**	-73.407	-37.608	11.5	N/A
	P14	**Valdivia**	-73.411	-39.844	10	N/A
	P15	**Ancud**	-73.828	-41.859	12	N/A
	P16	**Chiloe**	-74.176	-42.465	10	9
	P17	**Guafo**	-74.83	-43.578	10	10.2

6. Conclusions

The calculation of the flooding that a tsunami causes inland is addressed when a tsunami risk assessment is conducted. For a historical event, the assessment determines the limit of the affected area. In addition, the predictive evaluation of this flooded area, based on the potential tsunami scenarios that can affect it, allows prevention and mitigation measures to be established, helping to reduce the risk.

However, the calculation of this flooded area, particularly the assessment of the run-up, is not always direct. Occasionally, there are no high-resolution data that allow the application of numerical models. In addition, the accuracy of the existing empirical formulae can be improved, since they do not take into account natural topobathymetric profiles from the propagation to the inundation areas.

In this paper, an alternative methodology that complements the existing ones has been presented. This methodology consists of a numerical flume formed by the coupling of two numerical models (COMCOT and IH2VOF). The developed hybrid model is applied to each part of the generation-propagation-inundation process and this numerical model obtains a more accurate result; additionally, it is computationally affordable. The inputs for this hybrid model are the topobathymetric profile and the tsunami wave. The topobathymetric profiles were parameterized with 5 parameters (3 slopes and 2 depths), using a real profile sample to define the parameterization. In addition, the tsunami waves were parameterized with 2 parameters (tsunami height and period) using tsunami amplitude time series obtained by using numerical simulations of realistic tsunami events.

This methodology allows the accurate calculation of the run-up on along topobathymetric profile. Therefore, this methodology has been used to construct a tsunami run-up database. This database aimed to create an interpolation domain in which new run-up calculations could be carried out. The events of the database are combinations of a selection of bathymetric profiles and tsunami waves that were simulated with the hybrid model to create the database of simulations from which an interpolation can be executed to calculate the run-up of new tsunami scenarios.

To easily address the interpolation, a tool called IH-TRUST was scripted. This tool uses real profile and wave data, parameterizes them to find their most similar parameters in the database, and interpolates the results to provide a run-up value. Once the input parameters are given, the application of this interpolation provides results in just a few seconds, what shortens typical simulations of several nested grids, which commonly take several hours to provide results in all the computational domain.

To validate this new methodology and tool, the results of its application have been compared with both high-resolution numerical simulations and field survey data. The run-ups obtained with IH-TRUST are consistent and suggest that the tool can accurately calculate the run-up.

The assessment of the tsunami hazard begins by calculating the area affected by the tsunami. In those coastal areas where no other data are available, the detailed methodology and tool allow the run-up value of tsunami events to be determined without using high-resolution numerical simulations.

Therefore, to assess the hazard in a tsunami-prone area, this methodology can be applied to several profiles along the coastal area study. As a result, the methodology provides the run-up at each of the profiles, allowing an estimation of the flooded area from an area within the envelope of the run-up limits.

The application of the tool has some limitations; for example, the tool will indicate if the bathymetric profile or the tsunami wave parameters are not included within the range of values in the database, as explained for the case of Chilean Trench in 5.2.1.

New work in this field should take into account these difficulties to further develop the database with new parameter values that include these singularities.

The generation of the database and the values of run-up obtained from a combination of the bathymetric profiles and tsunami waves have provided a rich and populated space where the influence of each parameter on the final value of the run-up can be addressed. In this sense, which profiles are more prone to suffer higher run-ups in the case of a tsunami can be defined. For instance, profiles with high land slopes ($tan\beta_0$) are associated with higher run-up values than those with low land slopes. In addition, some combinations of offshore slopes and continental shelf slopes ($tan\beta_1$ and $tan\beta_2$) minimize the run-up value for the same tsunami wave. In addition, the influence of $tan\beta_2$ is considerable and justifies inclusion of the deep-water area (d_2) in the parameterized profile. On the other hand, when the profile is for a large continental shelf, the run-up increases; however, the run-up value decreases for gentle continental shelf slopes.

Traditionally, empirical methods, like the application of Synolakis´s formula, simplify the profile using one or two slopes (Park et al., 2015). However, this assumption is not accurate; in this study, the importance of using a complete profile, including the tsunami generation area, has been noted, as well as the influence of the profile parameters on the final run-up value.

Acknowledgements

The research leading to these results has received funding from the European Union's Seventh Framework Programme (FP7/2007-2013) under grant agreement n° 603839 (Project ASTARTE - Assessment, Strategy and Risk Reduction for Tsunamis in Europe).

Appendix A

Database profiles

In this section, the 49 artificially generated profiles are shown in Figure A1. The five corresponding parameters are listed on Table A1.

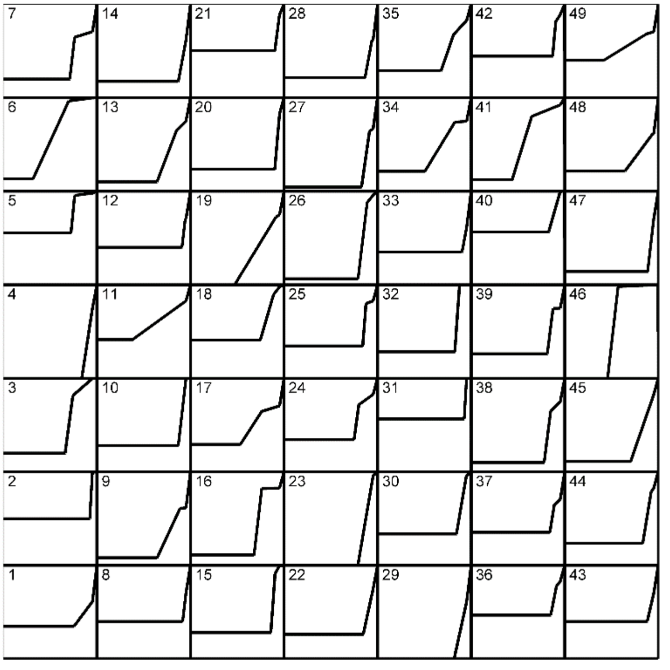

Fig. A1. The 49 profiles used to generate the IH-TRUST database

Table A1. Synthetic profiles

#	**tanβ_0**	**tanβ_1**	**tanβ_2**	***d_1***	***d_2***
1	15.00%	2.50%	2.50%	0	2600
2	0.05%	20.00%	20.00%	0	3000
3	0.05%	1.00%	8.50%	1100	4800
4	8.00%	10.00%	10.00%	0	6000
5	0.50%	0.15%	12.00%	150	2600
6	0.05%	0.15%	2.50%	200	5200
7	10.00%	0.50%	14.00%	500	4300
8	10.00%	14.00%	14.00%	0	2600
9	15.00%	0.15%	4.00%	50	5200
10	0.05%	10.00%	10.00%	0	4300
11	5.00%	1.00%	1.00%	0	3000
12	10.00%	0.50%	14.00%	20	2600
13	8.00%	1.50%	4.00%	800	5200
14	15.00%	10.00%	10.00%	0	4300
15	0.05%	2.00%	16.00%	500	4300
16	5.00%	0.05%	12.00%	50	5200
17	10.00%	0.50%	2.50%	500	3500
18	0.50%	1.50%	4.00%	500	3500
19	8.00%	1.00%	2.50%	200	6000
20	5.00%	16.00%	16.00%	0	4300

21	3.00%	10.00%	10.00%	0	2600
22	8.00%	7.00%	7.00%	0	3900
23	1.00%	7.00%	7.00%	0	6000
24	5.00%	1.00%	10.00%	800	3500
25	5.00%	0.50%	18.00%	200	3500
26	1.00%	1.50%	10.00%	500	5600
27	12.00%	1.00%	12.00%	200	5600
28	15.00%	0.30%	10.00%	20	3900
29	15.00%	8.50%	8.50%	0	6000
30	1.00%	1.00%	7.00%	20	3900
31	0.05%	2.50%	20.00%	20	2600
32	0.05%	0.05%	16.00%	20	4300
33	15.00%	10.00%	10.00%	0	2600
34	8.00%	0.15%	2.50%	100	4300
35	5.00%	1.50%	4.00%	1100	3900
36	5.00%	1.50%	7.00%	300	2600
37	10.00%	1.50%	10.00%	500	3000
38	8.00%	1.50%	12.00%	800	5200
39	8.00%	0.05%	12.00%	20	3900
40	0.05%	4.00%	4.00%	0	2600
41	2.00%	0.50%	4.00%	800	5200
42	3.00%	2.00%	14.00%	500	3000
43	10.00%	7.00%	7.00%	0	2600
44	5.00%	2.00%	8.50%	300	4300
45	5.00%	4.00%	4.00%	0	5200
46	0.05%	0.05%	10.00%	100	6000
47	10.00%	14.00%	14.00%	0	4800
48	15.00%	0.30%	2.50%	20	3900
49	10.00%	0.50%	1.00%	200	2600

References

Álvarez-Gómez, J. A., Aniel-Quiroga, Í., Gutiérrez-Gutiérrez, O. Q., Larreynaga, J., González, M., Castro, M., Gavidia, F., Aguirre-Ayerbe, I., González-Riancho, P. and Carreño, E.: Tsunami hazard assessment in El Salvador, Central America, from seismic sources through flooding numerical models., Nat. Hazards Earth Syst. Sci., 13(11), 2927–2939, doi:10.5194/nhess-13-2927-2013, 2013.

Aniel-Quiroga, Í., Alvarez-Gómez, J. A., González, M., Aguirre-Ayerbe, I., Fernández, F., Jara, M. S., González-Riancho, P., Medina, R. and Al-Yahyai, S.: Tsunami Hazard assessment and scenarios database development for the tsunami warning system for the coast of Oman, in international conference on reducing tsunami risk in the western Indian ocean, Muscat, Omán., 2015.

Baldock, T. E., Cox, D., Maddux, T., Killian, J. and Fayler, L.: Kinematics of breaking tsunami wavefronts: A data set from large scale laboratory experiments, Coast. Eng., 56(5–6), 506–516, doi:10.1016/J.COASTALENG.2008.10.011, 2009.

Barrientos, S. E. and Ward, S. N.: The 1960 Chile earthquake: inversion for slip distribution from surface deformation, Geophys. J. Int., 103(3), 589–598, doi:10.1111/j.1365-246X.1990.tb05673.x, 1990.

Bathymetry Consortium EMODnet: EMODnet Digital Bathymetry (DTM). EMODnet Bathymetry, Mar. Inf. Serv., doi:http://doi.org/10.12770/c7b53704-999d-4721-b1a3-04ec60c87238, 2016.

Battjes, J. A.: SURF SIMILARITY, in Coastal Engineering Proceedings, vol. 1., 1974.

Camus, P., Mendez, F. J. and Medina, R.: A hybrid efficient method to downscale wave climate to coastal areas, Coast. Eng., 58(9), 851–862, doi:10.1016/j.coastaleng.2011.05.007, 2011.

Carrier, G. F. and Greenspan, H. P.: Water waves of finite amplitude on a sloping beach, J. Fluid Mech., 4(1), 97–109, doi:10.1017/S0022112058000331, 1958.

Chan, I.-C. and Liu, P. L.-F.: On the runup of long waves on a plane beach, J. Geophys. Res. Ocean., 117(C8), n/a-n/a, doi:10.1029/2012JC007994, 2012.

Fritz, H. M., Petroff, C. M., Catalán, P. A., Cienfuegos, R., Winckler, P., Kalligeris, N., Weiss, R., Barrientos, S. E., Meneses, G., Valderas-Bermejo, C., Ebeling, C., Papadopoulos, A., Contreras, M., Almar, R., Dominguez, J. C. and Synolakis, C. E.: Field Survey of the 27 February 2010 Chile Tsunami, Pure Appl. Geophys., 168(11), 1989–2010, doi:10.1007/s00024-011-0283-5, 2011.

Fuentes, M. A., Ruiz, J. A. and Riquelme, S.: The runup on a multilinear sloping beach model, Geophys. J. Int., 201(2), 915–928, doi:10.1093/gji/ggv056, 2015.

Fuhrman, D. R. and Madsen, P. A.: Surf Similarity and Solitary Wave Runup, J. Waterw. Port, Coastal, Ocean Eng., 134(3), 195–198, doi:10.1061/(ASCE)0733-950X(2008)134:3(195), 2008.

Garcia, N., Lara, J. L. and Losada, I. J.: 2-D numerical analysis of near-field flow at low-crested permeable breakwaters, Coast. Eng., 51(10), 991–1020, doi:10.1016/J.COASTALENG.2004.07.017, 2004.

Hsu, T.-J., Sakakiyama, T. and Liu, P. L.-F.: A numerical model for wave motions and turbulence flows in front of a composite breakwater, Coast. Eng., 46(1), 25–50, doi:10.1016/S0378-3839(02)00045-5, 2002.

Hunt, I. A.: Design of seawalls and brekwaters, J. Wtrwy. Harb. Div., 85, 123–152, 1959.

IHCantabria: Evaluación probabilística de la peligrosidad y la vulnerabilidad frente a desastres naturales basados en proyecciones de cambio climático en el área metropolitana de Trujillo. [online] Available from: https://studylib.es/doc/8407409/resumen_ejecutivo_trujillo-y-minam, 2013.

International Hydrographic Organization: General Bathymetric Chart of the Oceans., 2014.

Iribarren, R. and Nogales, C.: Protection des Ports, in 17th Int. Navigation Congress, Section II, Lisbon, pp. 31–80., 1949.

Jacobsen, N. G., Fuhrman, D. R. and Freds??e, J.: A wave generation toolbox for the open-source CFD library: OpenFoam??, Int. J. Numer. Methods Fluids, 70(9), 1073–1088, doi:10.1002/fld.2726, 2012.

Kanamori, H. and Anderson, D. L.: Importance of physical dispersion in surface wave and free oscillation problems: Review, Rev. Geophys., 15(1), 105, doi:10.1029/RG015i001p00105, 1977.

KÂNOĞLU, U. and SYNOLAKIS, C. E.: Long wave runup on piecewise linear topographies, J. Fluid Mech., 374, S0022112098002468, doi:10.1017/S0022112098002468, 1998.

Keller, J. and Keller, H.: Water wave run-up on a beach, Off. Nav. Res. Dep. Navy, 40 [online] Available from: http://oai.dtic.mil/oai/oai?verb=getRecord&metadataPrefix=html&identifier=AD0608864, 1964.

Kobayashi, N. and Karjadi, E. A.: Surf Similarity Parameter for Breaking Solitary-Wave Runup, J. Waterw. Port, Coastal, Ocean Eng., 120(6), 645–650, doi:10.1061/(ASCE)0733-950X(1994)120:6(645), 1994.

Lara, J. L., Garcia, N. and Losada, I. J.: RANS modelling applied to random wave interaction with submerged permeable structures, Coast. Eng., 53(5), 395–417, doi:10.1016/j.coastaleng.2005.11.003, 2006.

Li, Y. and Raichlen, F.: SOLITARY WAVE RUNUP ON PLANE SLOPES, [online] Available from: http://ascelibrary.org/doi/pdf/10.1061/(ASCE)0733-950X(2001)127:1(33) (Accessed 16 November 2017), 2001.

Lin, P. and Liu, P. L.-F.: A numerical study of breaking waves in the surf zone, J. Fluid Mech, 359, 239–264, 1998.

Lomnitz, C.: Major Earthquakes of Chile: A Historical Survey, 1535-1960, Seismol. Res. Lett., 75(3), 368–378, doi:10.1785/gssrl.75.3.368, 2004.

Madsen, P. A. and Schäffer, H. A.: Analytical solutions for tsunami runup on a plane beach: single waves, N-waves and transient waves, J. Fluid Mech., 645, 27, doi:10.1017/S0022112009992485, 2010.

Madsen, P. A., Fuhrman, D. R. and Scha, H. A.: On the solitary wave paradigm for tsunamis, J. Geophys. Res., 113(December), doi:10.1029/2008JC004932, 2008.

Meinig, C., Stalin, S. E., Nakamura, A. I. and Milburn, H. B.: Real-Time Deep-Ocean Tsunami Measuring, Monitoring, and Reporting System: The NOAA DART II Description and Disclosure. [online] Available from: http://www.ndbc.noaa.gov/dart/dart_ii_description_6_4_05.pdf (Accessed 26 November 2017), 2005.

National Geophysical Data Center NOAA.: National Geophysical Data Center / World Data Service (NGDC/WDS): Global Historical Tsunami Database., , doi:doi:10.7289/V5PN93H7, n.d.

Okada, Y.: Surface deformation due to shear and tensile faults in a half-space Okada, Y Bull Seismol Soc AmV75, N4, Aug 1985, P1135–1154, Int. J. Rock Mech. Min. Sci. Geomech. Abstr., 75, 1135–1154, doi:10.1016/0148-9062(86)90674-1, 1985.

Papadopoulos, G.: Tsunamis in the European-Mediterranean Region., 2016.

Park, H., Cox, D. T., Petroff, C. M., Park, H., Cox, D. T. and Petroff, C. M.: An empirical solution for tsunami run-up on compound slopes, Nat Hazards, 76, 1727–1743, doi:10.1007/s11069-014-1568-7, 2015.

Pengzhi Lin, B. and L-F Liu, P.: INTERNAL WAVE-MAKER FOR NAVIER-STOKES EQUATIONS MODELS, [online] Available from: https://ascelibrary.org/doi/pdf/10.1061/%28ASCE%290733-950X%281999%29125%3A4%28207%29 (Accessed 13 March 2018), 1999.

Riquelme, S., Fuentes, M., Hayes, G. P. and Campos, J.: A rapid estimation of near-field tsunami runup, J. Geophys. Res. Solid Earth, 120(9), 6487–6500, doi:10.1002/2015JB012218, 2015.

Selva, J., Tonini, R., Molinari, I., Tiberti, M. M., Romano, F., Grezio, A., Melini, D., Piatanesi, A., Basili, R. and Lorito, S.: Quantification of source uncertainties in Seismic Probabilistic Tsunami Hazard Analysis (SPTHA), Geophys. J. Int., 205(3), 1780–1803, doi:10.1093/gji/ggw107, 2016.

Sepúlveda, I. and Liu, P. L.-F.: Estimating tsunami runup with fault plane parameters, Coast. Eng., 112, 57–68, doi:10.1016/j.coastaleng.2016.03.001, 2016.

Shao, G., Li, X., Zhao, X., Yano, T. and Ji, C.: Result for Rupture Process of Feb 27, 2010 Mw 8.86 Chile Earthquake, [online] Available from: http://www.geol.ucsb.edu/faculty/ji/big_earthquakes/2010/02/27/chile_2_27.html (Accessed 21 November 2017), 2010.

Synolakis, C. E.: The runup of solitary waves, J. Fluid Mech., 185(1), 523, doi:10.1017/S002211208700329X, 1987.

Titov, V. V, Moore, C. W., Greenslade, D. J. M., Pattiaratchi, C., Badal, R., Synolakis, C. E., Nog, U. K. and Lu, ˘: A New Tool for Inundation Modeling: Community Modeling Interface for Tsunamis (ComMIT), Pure Appl. Geophys., 168, 2121–2131, doi:10.1007/s00024-011-0292-4, 2011.

UNESCO-IOC: Tsunami risk assessment and mitigation for the Indian Ocean; knowing your tsunami risk – and what to do about it, , (June), Manuals and guides 52, 2009.

Wang, X.: COMCOT User Manual Ver. 1.7, Cornell Univ., 6, 1–59, 2009.